ENVELOPE ANALYSIS OF INTENSE RELATIVISTIC QUASI-LAMINAR BEAMS IN RF PHOTOINJECTORS: A THEORY OF EMITTANCE COMPENSATION

Luca Serafini
INFN - Milan, Via Celoria 16 - 20133 Milano - Italy
James B. Rosenzweig
Department of Physics and Astronomy - University of California, Los Angeles
405 Hilgard Avenue, Los Angeles, CA 90095-1547

ABSTRACT

In this paper we provide an analytical description for the transverse dynamics of relativistic, space charge-dominated beams undergoing strong acceleration, such as those typically produced by RF photoinjectors. These beams are chiefly characterized by a fast transition, due to strong acceleration, from the non-relativistic to the relativistic regime in which the initially strong collective plasma effects are greatly diminished. However, plasma oscillations in the transverse plane are still effective in significantly perturbing the evolution of the transverse phase space distribution, introducing distortions and longitudinal-transverse correlations that cause an increase in the rms transverse emittance of the beam as a whole. The beam envelope evolution is dominated by such effects and not by the thermal emittance, and so the beam flow can be considered quasi-laminar.

The model adopted is based on the rms envelope equation, for which we find an exact particular analytical solution taking into account the effects of linear space charge forces, external focusing due to applied as well as ponderomotive RF forces, acceleration and adiabatic damping, in the limit that the weak non-laminarity due to the thermal emittance may be neglected. This solution, termed the invariant envelope, represents a special mode for beam propagation which assures a secularly diminishing normalized rms emittance and it represents the fundamental operating condition of a space-charge

compensated RF photoinjector. The conditions for obtaining emittance compensation in a long, integrated photoinjector, in which the gun and linac sections are joined, as well as in the case of a short gun followed by a drift and a booster linac, are examined.

PACs Nos: 41.75 -i , 41.85 -p , 29.17 +w , 29.25 Bx , 29.27 Bd

Submitted to Physical Review E

I. INTRODUCTION

Quasi-laminar, space charge-dominated relativistic electron beams have become a subject of great interest with the advent of short laser pulse-driven radio-frequency (RF) photoinjectors [1,2], which are able to produce electron beams carrying current densities well in excess of 1 kA/cm^2, with the transition from the non-relativistic to the relativistic regime occurring very quickly. The accelerating gradient required to guarantee that the beam will be captured in the RF wave at relevant wavelengths (5-25 cm) ranges from 10 MeV/m up to 100 MeV/m: the beam is therefore accelerated from rest at the photocathode emissive surface, up to relativistic energy within a fraction of an RF wavelength, which is a distance is comparable to one-half of a plasma oscillation period in the transverse plane. The trapping condition is typically expressed as $\alpha > 1/2$, in terms of the quantity $\alpha = eE_0/2kmc^2$, which represents the dimensionless amplitude of the vector potential associated to the accelerating field, of frequency ν_{RF} ($k = 2\pi\nu_{RF}/c$) and amplitude E_0.

Furthermore, the random, thermal component to the transverse emittance is very small compared to the total rms emittance, which is dominated by the dilution of the projected transverse phase space density due to correlations in the beam distribution

function, so that the beam is fairly laminar both in the transverse and the longitudinal planes. This implies that in the transverse plane trajectories do not cross each other, while in the longitudinal plane different slices (of length small compared to the total bunch length) do not mix with each other. Since neighbouring longitudinal slices additionally do not behave in vastly different ways, precluding the occurrence of large longitudinal density gradients in the beam charge density, this final condition implies that the beam may be broken up, for analysis purposes, into nearly independent longitudinal slices which behave in the same manner as a continuous beam. Evidence for the validity of this model for photoinjector beam dynamics comes from both multiparticle simulations, and from experiments performed at Brookhaven by Wang, *et al.*[3] .

This set of conditions, which defines the notion of a quasi-laminar beam in this paper, is generally attained in RF photoinjectors, in particular when they are operated in the space-charge emittance compensation regime[4]. This regime implies that the beam propagates for one transverse plasma oscillation, so that the correlations in the transverse phase space which develop in the first half of the oscillation are undone in the second half by properly focusing the beam. Due to the relativistic diminishing of the space charge forces as the beam accelerates, one can adiabatically nearly terminate the plasma motion and associated emittance oscillations as the minimum in the emittance occurs, obtaining maximum beam brightness at the exit of the photoinjector.

In this paper we wish to provide a simple frame work in which the beam dynamics in such a regime can be analytically described and the space-charge emittance correction technique can be quantitatively explained. We begin by using an heuristic model of the plasma and emittance oscillations in a quasi-laminar beam. This model allows the underlying physical mechanisms involved in the complicated phase space dynamics of the RF photoinjector to be elucidated. After this discussion, we then construct the quantitative model for quasi-laminar beam propagation. Analytical expressions for the beam envelope from the photocathode surface up to the gun exit in a long, integrated RF photoinjector are

provided and the predictions for optimum photoinjector configuration to achieve emittance correction are extracted from the properties of the envelope itself. A particular solution for the beam envelope is found that assures all the bunch slices evolve in transverse space phase with a common phase space angle, which is in fact the desired final state to achieve emittance compensation. This particular solution is termed the invariant envelope, and is in many ways analogous to the equilibrium Brillouin flow of space charge dominated beams in constant gradient focusing channels. Although this study is directly applied to a description of RF photoinjectors, the concept of invariant envelope and the method of analysis is of interest and applicable to any relativistic beam which is space-charge dominated and accelerated in high gradient linear accelerators.

The equation we base our analysis on is Lawson's expression for the evolution of the rms envelope in the paraxial limit[5],

$$\sigma'' + \sigma'\left(\frac{\gamma'}{\beta\gamma}\right) + K_r\sigma - \frac{\kappa_s}{\sigma\beta^3\gamma^3} - \frac{\varepsilon_n^2}{\sigma^3\beta^2\gamma^2} = 0, \tag{1.1}$$

which governs the evolution of the cylindrical symmetric rms transverse beat spot size $\sigma(z)$ under the effects of an external linear focusing channel of strength $K_r \equiv -F_r/\beta^2\gamma mc^2$. Here the prime indicates differentiation with respect to the independent variable z, the distance along the beam propagation axis, γmc^2 is the mean beam energy and $\beta \equiv v_b/c = \sqrt{1-\gamma^{-2}}$ is the normalized mean beam velocity. The defocusing space charge term in Eq. 1.1 is proportional to the beam perveance κ_s, and final term represents the outward pressure due to the normalized rms emittance, which in the case of cylindrical symmetry can be written as

$$\varepsilon_n \equiv \beta\gamma\varepsilon = \frac{\beta\gamma}{2}\sqrt{\langle r^2\rangle\langle r'^2\rangle - \langle rr'\rangle^2}\,. \tag{1.2}$$

We use Eq. 1.1 under a host of assumptions, which we now delineate. Equation 1.1 is of course only valid in paraxial approximation ($\sigma' << 1$) and for a narrow energy spread beam. In our envelope analysis, which is applied only in the region where the beam has attained relativistic velocities (the mean beam velocity $v_b = \beta c \approx c$), the normalized acceleration gradient γ' is approximated as constant, so that $\gamma(z_2) = \gamma(z_1) + \gamma'(z_2 - z_1)$. In the case of an unbunched beam the perveance takes the form $\kappa_s = 2I/I_0$, with $I_0 = ec / r_e \cong 17$ kA (for electrons). Since we restrict the discussion to axisymmetric beams, the focusing gradient can incorporate two different types of focusing, that applied externally by a magnetostatic solenoidal focusing field, and the ponderomotive RF focusing[6] produced by the non-synchronous spatial harmonics of the accelerating RF wave, an effect which is particularly strong in a high gradient standing wave accelerator such as an RF photoinjector. As discussed in Refs. 6 and 7, these two focusing sources can be cast into a single expression

$$K_r = \left[\frac{\eta}{8} + b^2\right]\left(\frac{\gamma'}{\gamma \sin(\phi)}\right)^2, \tag{1.3}$$

where $b = cB_z / E_0$ ($eE_0 = 2\gamma' m_e c^2 / \sin(\phi)$, $\gamma' = \alpha k \sin(\phi)$) for the particular case of a constant solenoidal magnetic field, ϕ is the particle phase with respect to the RF field wave, $\phi = \omega t - kz + \phi_0$, and ϕ_0 is the RF phase of the bunch centroid at injection. The quantity η, which is a measure of the higher spatial harmonic amplitudes of the RF wave is defined in Section III and is generally quite close to unity in practical RF structures.

We have given the expression for the beam perveance in Eq. 1.1 above for an unbunched beam of constant current I. In our analysis of the quasi-laminar beam in Section III, we generalize this quantity to include the case of bunched beam, by incorporating a geometrical factor[8] $g(\zeta)$ in the perveance which contains the longitudinal

dependence of the transverse space charge field versus the internal bunch coordinate $\zeta = z - v_b t$.

Furthermore, Eq. 1.3 ignores possible chromatic aberration effects on the transverse phase space dynamics, due to an energy-phase correlation in the bunch — this analytical study is carried out assuming a monoenergetic bunch. A related source of longitudinal-transverse phase space correlations in this system arises from the phase dependence of the transverse RF forces, which gives rise to an emittance increase[9] at the first iris of the gun (*cf.* Figure 3). We assume that this source of emittance, like the chromatic effects, does not give rise to significant changes in the transverse beam dynamics of a given ζ-slice of the bunch. This assumption is quite good, in that these correlations are of a similar form to the those arising from space-charge, but smaller in magnitude in nearly all cases of interest. In fact, because of the similarity in spatial dependence of the forces, it has been observed in simulations that the space-charge emittance compensation process can also partially mitigate this source of emittance[10]. Although the solutions found for Eq. 1.1 can be extended to any kind of charge density distribution in the bunch, the actual predictions of the RF photoinjector designed to achieve emittance compensation will be provided for a density distribution which is Gaussian in all dimensions.

The initial model used for the photoinjector analysis assumes a long multi-cell RF structure, *i.e.* an integrated device such as the AFEL injector at Los Alamos[4], and the proposed PWT injector at UCLA[11]. The analysis is, however, sufficiently broad that many characteristics of photoinjectors with short (one or two cell) RF guns and a post-acceleration (booster) linac, where the space charge compensation takes place in drift space between the RF gun and the booster linac, can be inferred. In fact, the case of a short (1+1/2 cell) RF gun followed by a drift is discussed in Section VI. The exact solution for the beam envelope is not found for this case, but the operating conditions needed to achieve emittance compensation are deduced from the general properties of the envelope equation.

Radial nonlinearities in the space charge field are not taken into account in this model, as they have a weak impact on the rms envelope behaviour. The full influence of these effects are beyond the scope of this paper, but are important nonetheless - they are more relevant to a discussion of minimizing the residual emittance after compensation. Some comments on this subject are made in Section II.

In overview, the organization of the paper is as follows. In Section II we provide an heuristic model to explain the basics of the emittance oscillation due to a small mismatch of a space charge dominated beam at injection into focusing channel. Section III is devoted to the detailed analysis of the envelope equation and the model for a multi-cell photoinjectors; analytical solutions derived in a perturbative approximation around an exact solution are presented. The concept of the invariant envelope is introduced and illustrated in Section IV, and its deep relationship with the space charge emittance compensation technique is discussed. Predictions relevant to photoinjector design characteristics needed to achieve an invariant envelope operation, i.e. emittance compensation, are presented in Section V together with comparisons to numerical simulations of existing RF photoinjector designs. Section VI is devoted to the case of a short RF gun followed by a drift space where the emittance correction takes place. Finally, the implications of the analysis presented in this paper are summarized in Section VII.

II. AN ILLUSTRATIVE MODEL

The simplified model for the complicated motion of the beam envelope and emittance evolution in high gradient linear accelerators we propose is motivated primarily by the problem of understanding emittance evolution in RF photoinjector sources. In this model we view the rms emittance as arising from the differing phase space dynamics of each longitudinal slice of the beam which is assumed to behave as an independent, cold, laminar, space-charge dominated plasma evolving under the influence of linear external forces. In this case, even though the rms emittance of each longitudinal slice can be neglected in the analysis, the rms emittance of the ensemble can be quite large upon summation of the entire ensemble making up the beam.

In order to understand how this mechanism causes emittance growth, as well as how the emittance growth can be reversed by proper focusing of the beam, we begin by examining a simplified model problem, that of an intense, cold, uniform-density beam nearly matched to an external focusing channel. While this model ignores the effects of acceleration and transverse motion due to the high gradient RF fields in the accelerator, it serves to illuminate the fundamental dynamics of the emittance oscillations in these devices. When the effects of the high gradient electromagnetic fields are included in the subsequent analysis, analogies to this simple model will be apparent.

We begin by writing the rms envelope equation for a cylindrical symmetric, space charge dominated, coasting, relativistic, charged particle beam in a focusing channel of constant strength,

$$\sigma'' + K_r\sigma = \frac{2I}{I_0(\beta\gamma)^3\sigma} + \frac{\varepsilon_{n,th}^2}{(\beta\gamma)^2\sigma^3}. \qquad (2.1)$$

Given our assumption of space charge-dominated envelope motion, we may ignore the final term on the right hand side of Eq. 2.1, which represents the contributions to envelope forcing due to the emittance arising from both random, thermalizing sources as well as the effects of nonlinear macroscopic forces. In this analysis, we will be using Eq. 2.1 to describe the evolution of longitudinal slices of a beam (meaning infinitesimally small lengths $\delta\zeta$ of beam about given values of ζ), assuming that the motion of each slice is essentially uncorrelated to that of nearby slices, and in fact depends most strongly only the local (in ζ) value of the current. This means that the normalized thermal emittance corresponding to each beam slice, which we define formally as

$$\varepsilon_{n,th}(\zeta) \equiv \frac{\beta\gamma}{2}\sqrt{\langle r^2\rangle_\zeta \langle r'^2\rangle_\zeta - \langle rr'\rangle_\zeta^{\,2}}, \tag{2.2}$$

where the subscript ζ indicates that the average is performed only over the distribution within a given slice.

We next generalize the expression of for the space charge term to include an explicit dependence on the longitudinal position by $I \to Ig(\zeta)$, where I is now defined as the maximum current in the beam. The geometrical factor $g(\zeta)$, which is less than unity, is discussed in more detail for a finite beams below; for now let us note that in the limit that the beam is long ($\gamma\sigma_z >> \sigma_r$) in its rest frame $g(\zeta)$ follows the local dependence of the current very closely.

Upon linearizing Eq. 2.1 about the equilibrium Brillouin flow condition for a slice at a given value of ζ,

$$\sigma_{eq}(g(\zeta)) = \sqrt{\frac{2Ig(\zeta)}{I_0(\beta\gamma)^3 K_r}}, \tag{2.3}$$

we obtain the equation for small amplitude motion about this point,

$$\delta\sigma''(\zeta)+\left[K_r+\frac{2Ig(\zeta)}{I_0(\beta\gamma)^3\sigma_{eq}^2 g(\zeta)}\right]\delta\sigma(\zeta)=0 \quad \text{or}$$
$$\delta\sigma''(\zeta)+2K_r\delta\sigma(\zeta)=0. \tag{2.4}$$

which gives oscillation frequencies which are dependent on the external focusing strength, but *independent* of the beam current. It is this characteristic of the space charge dominated, quasi-laminar beam dynamics that allows emittance compensation.

This model can be used to illuminate the RF photoinjector case by assuming that the envelopes in the beam ensemble begin (at the "cathode") slightly mismatched to the channel with $\sigma=\sigma_0<\sigma_{eq}$ and $\sigma'=0$. All envelope oscillations proceed with the same frequency, given only by the external focusing strength, but with different amplitude and about equilibria which are dependent on the current (if we assume the approximation that $g(\zeta)$ is proportional to the current). We thus have formally

$$\sigma(z,\zeta)=\sigma_{eq}(g(\zeta))+(\sigma_0-\sigma_{eq}(g(\zeta)))\cos(\sqrt{2K_r}z), \quad \text{and} \tag{2.5}$$

$$\sigma'(z)=-\sqrt{2K_r}(\sigma_0-\sigma_{eq}(g(\zeta)))\sin(\sqrt{2K_r}z). \tag{2.6}$$

Since the frequency of the oscillations is independent of the value of current, but the amplitude is not, the rms emittance of the beam ensemble grows, but returns periodically to minimum values.

This can be seen by noting that under our above assumptions, the rms emittance defined by Eq. 1.2 can be calculated as follows,

$$\varepsilon(z)=\sqrt{\langle\sigma^2\rangle\langle\sigma'^2\rangle-\langle\sigma\sigma'\rangle^2}, \tag{2.7}$$

where the bracket indicates an average weighted over the distribution of currents in the entire beam ensemble, *i.e.* all of the slices. To quantify the effect of the differing trajectories in the ensemble of beam slices, we assume the long beam limit expand the effective distribution function in currents to second order about the maximum current (*i.e.* near the peak of a symmetric beam current profile which is continuous though its first ζ-derivative), and obtain the emittance evolution

$$\begin{aligned}\varepsilon(z) &\cong \frac{1}{\sqrt{2}}\sigma_0(\delta I_{\mathrm{rms}})\left|\frac{\partial}{\partial I}\left(\frac{\sigma'}{\sigma}\right)\right|_{I=I_p} \\ &\cong \frac{1}{2}\sqrt{K_r}\sigma_0\sigma_{eq}(I_p)\frac{\delta I_{\mathrm{rms}}}{I_p}\left|\sin\left(\sqrt{2K_r}z\right)\right|.\end{aligned} \tag{2.8}$$

Figure 1 displays the emittance and envelope evolution for a slightly mismatched beam ensemble, beginning, as in the case of the RF photoinjector, with a minimum beam size and vanishing emittance as defined by Eq. 2.7. It can be seen that there are two subsequent emittance null points, one at the maximum in beam size, and another when it returns to its original size. These minima occur where the angles in phase space $\theta = \tan^{-1}(\sigma'/\sigma)$ are independent of the beam current value. This type of behaviour is in fact similar to that observed in RF photoinjectors, as is can be seen from the multi-particle simulation shown in Figure 2, where the beam undergoes one envelope oscillation and two emittance oscillations from the cathode to the injector end in the UCLA Saturnus photoinjector. The emittance minimum occurring at the maximum in the envelope is of secondary interest because it occurs at large beam size and low energy inside of the primary focusing magnet of the RF photoinjector.

The qualitative similarity between the behaviour predicted by simple emittance oscillation model and that found in simulation of RF photoinjectors points the way toward the further analysis of the photoinjector, which differs from the model case in both acceleration and nonuniform application of focusing. One prediction can be gleaned from

the simple model even before we begin, which is that one should allow the photoinjector beam to go through only one envelope oscillation, with further oscillations suppressed by diminishing the space charge forces through acceleration. This must be done with some care, and our analysis leads eventually to a quantitative prescription for obtaining this condition in Section V.

This simple model has other aspects which help explain by analogy the behaviour of RF photoinjectors operated in the emittance compensation regime. The artefact of the oscillation frequency about the equilibrium being dependent only on the applied restoring force gradient, which is what allows the correlated emittance developing in the beam ensemble to periodically vanish, is not valid for all amplitudes in the beam envelope system. To lowest significant order in the mismatch amplitude $a(I(\zeta)) = (\sigma_0 - \sigma_{eq}(I(\zeta)))/\sigma_{eq}(I(\zeta))$, the oscillation frequency is

$$\nu(I(\zeta)) = \sqrt{2K_r}\left[1 + \tfrac{3}{16}a(I(\zeta))^2\right]. \tag{2.9}$$

This anharmonicity in the beam ensemble generally precludes the vanishing of the correlated emittance. Thus, there is an additional prediction that can be made on the basis of this observation: excursions in the beam size should be minimized to produce the best emittance compensation.

It should also be noted that, assuming laminarity (there is no "wave-breaking" in transverse phase space) within a longitudinal beam slice is maintained, that phase space correlations arising from radial nonlinearities must also behave as do the beam slices - that is they should also be compensated. Maintenance of laminarity also implies that the beam excursions from equilibrium be limited in amplitude.

III. BEAM ENVELOPE ANALYSIS FROM CATHODE SURFACE TO INJECTOR EXIT

In order to perform the envelope analysis of the multi-cell injector presented below, we must first specify a model for the RF photoinjector. The model we adopt for the accelerating structure is geometry-independent, since the accelerating RF field is written in a Floquet form as a sum of its spatial harmonic amplitudes, and the RF photoinjector cavity is assumed to be a multi-cell structure indefinitely extending along its symmetry axis. There is however some specificity in our choice of the model for the static longitudinal magnetic field produced by the external focusing solenoids: it is assumed to have a hard-edge longitudinal profile extending over a few cells of the accelerating structure.

A typical multi-cell RF cavity employed in RF photoinjectors is shown in Fig. 3, displaying the cross section of an axisymmetric iris-loaded structure terminated into a half cell hosting the cathode (located at $z = 0$) and operated in a $TM_{010-\pi}$ standing mode with one-half wavelength cells following the cathode cell. The general expression of the RF field components expanded linearly off-axis is[6]:

$$\begin{aligned} E_z &= E_0 \sum_{n=1,odd}^{\infty} a_n \cos(nkz)\sin(\omega t + \phi_0) \quad ; \\ E_r &= \frac{kr}{2} E_0 \sum_{n=1,odd}^{\infty} n \cdot a_n \sin(nkz)\ \sin(\omega t + \phi_0) \quad ; \\ B_\theta &= c\frac{kr}{2} E_0 \sum_{n=1,odd}^{\infty} a_n \cos(nkz)\cos(\omega t + \phi_0) \quad ; \end{aligned} \tag{3.1}$$

where $k = 2\pi/\lambda = \omega/c$, and a_n are the spatial harmonic coefficients which depends on the actual cavity geometry which can be easily computed by computer codes or derived by experimental bead measurements. Due to the symmetry of the selected mode, all even a_n's vanish, $a_1 = 1$, and E_0 becomes the amplitude of the fundamental harmonic (speed-of-light

phase velocity) component of the RF wave. All higher harmonic amplitudes are therefore normalized to the value of the fundamental.

The external solenoid is assumed to be folded around the first 2+1/2 cells of the RF cavity, producing a constant magnetic field $B_z = B_0$ from $z_b = \lambda / 8$ (half way through the cathode cell) up to $z_c = 11\lambda / 8$ (a quarter way through the third full cell). The beam dynamics in the photoinjector are described using a three stage procedure:

a) The first one and one-half cells (from $z = 0$ to $z = z_2$) are treated by using a ballistic approximation, as described in Ref. 7. In this region the transverse plasma oscillation begins, driven by the strongly repulsive space charge forces. The transverse dynamics are dominated by the defocusing effects of space charge and a transient RF kick in the region of the first iris.

b) In the following cells, i.e. up to the end of the solenoid field at $z = z_c$, the envelope equation is solved perturbatively with a constant beam size space charge approximation. Here, the extra focusing applied by the solenoid field, in conjunction with the ponderomotive RF focusing, overcomes the transverse space charge force and turns the beam envelope from divergent to convergent.

c) In the final region of the accelerator (beyond $z = z_c$), the envelope equation is solved initially as perturbation about an approximate solution, which provides a general solution to the problem of the beam dynamics up to the end of the photoinjector. In the case of a nearly optimized injector, this approximate solution can be replaced by a special exact solution called invariant envelope. In this case, the normalized emittance associated with the perturbed plasma oscillations is damped gently for a beam nearly matched to the invariant envelope, while it can be excited to perform additional oscillations if the beam is overfocused by the solenoid, going through successive minima and maxima.

The beam conditions σ_2 and σ_2' at the second iris, *i.e.* at the end of the first region, are reported in Appendix A ($\gamma_2 = 1 + 3\pi\alpha / 2$ at $\phi = \pi/2$). With the condition $\alpha > 1/2$, the trapping threshold requirement which holds for any RF photoinjector[9], the

beam at this point is quite relativistic, since typically $\gamma_2 \cong 5-10$. Rewriting the envelope equation assuming $\beta \cong 1$ and beam laminarity (neglecting the thermal emittance), Eq. 1.1 becomes

$$\sigma'' + \sigma' \frac{\gamma'}{\gamma} + \sigma\left(\frac{\eta}{8} + b^2\right)\left(\frac{\gamma'}{\gamma \sin(\varphi)}\right)^2 = \frac{\kappa_s(\zeta)}{\sigma\gamma^3}, \tag{3.2}$$

where the normalized beam energy is given to excellent approximation by $\gamma = 1 + \alpha kz\sin(\phi) + \alpha\cos(\phi) \cong 1 + \gamma' z + \alpha\cos(\phi)$, and we now leave out the explicit indication of the dependence of σ on ζ and z. The ponderomotive RF focusing term displays, through the quantity η, its dependence on the higher spatial harmonic amplitudes[6],

$$\eta = \sum_{n=1}^{\infty} a_{n-1}^2 + a_{n+1}^2 - 2a_{n-1}a_{n+1}\cos(\phi) \quad (a_0 = 0). \tag{3.3}$$

In Eq. 3.2 the perveance $\kappa_S(\zeta)$ explicitly retains a functional dependence on the longitudinal position ζ of the particular slice in the bunch, so that $\kappa_S(\zeta) = 2Ig(\zeta)/I_0$. As shown through more detailed calculations in Appendix B, the geometric factor $g(\zeta)$ is given by $g(\zeta) = e^{-\frac{\zeta^2}{2\sigma_z^2}}\left\{1 + \frac{A^2}{\gamma^2}\left[\left(1 - \frac{\zeta^2}{\sigma_z^2}\right)\left(\frac{1}{2} + \ln\left(\frac{A}{\gamma}\right)\right) - 1\right]\right\}$ for a Gaussian distribution of aspect ratio $A = \sigma_r / \sigma_z$, or $g(\zeta) = 1 - \frac{2A^2}{\gamma^2}\left[1 + 12\left(\frac{\zeta}{L}\right)^2 + 80\left(\frac{\zeta}{L}\right)^4\right]$ for a uniform distribution of aspect ratio $A = R/L$, where R is the beam radius and L is the beam length. In this section we will assume, for sake of simplicity, $g(\zeta) \cong I(\zeta)/I_{peak}$, so that $\kappa_S(\zeta)$ does not depend on γ; which is consistent with the relativistic approximation that the transverse space charge field amplitude follow the beam current distribution. As a matter of fact, since the bunch aspect ratio A is typically of the order of 1, the rest frame

aspect ratio is such that $A^2/\gamma^2 << 1$ in the domain where Eq. 3.2 is applied ($\gamma > \gamma_2$). However, the generalization of the Eq. 3.2 to deal with analysis of bunched beam dynamics will be performed in following sections, together with the analysis of the emittance compensation mechanism.

To solve Eq. 3.2, we apply a Cauchy transformation by changing the independent variable from z to y, defined as $y \equiv \ln(\gamma/\gamma_2)$, to obtain

$$\frac{d^2\sigma}{dy^2} + \Omega^2\sigma = \frac{S(\zeta)}{\sigma}e^{-y}, \tag{3.4}$$

with $\sigma = \sigma(y)$ and $S(\zeta) \equiv 2I(\zeta)/I_0\gamma_2\gamma'^2 = \kappa_s(\zeta)/\gamma_2\gamma'^2$ defined to be the Cauchy perveance. We obtain solutions to Eq. 3.4 employing two different techniques appropriate to two distinct domains of propagation. In the first region, defined by $z_2 < z < z_c$ ($0 < y < y_c$) with $y_c = \ln[(1+(5/2+1/4)\pi\alpha)/\gamma_2]$, the beam is exposed to external solenoidal focusing. In this domain we have $\Omega^2 = \left(\eta/8 + b^2\right)/\sin^2(\phi)$, where $b = cB_0/E_0$. The second domain, $z > z_c$, is solenoid free and hence $\Omega = \Omega_0 = \left(\eta/\sqrt{8}\right)\sin(\phi)$. In the first domain the beam size σ varies slightly with respect to σ_2, allowing the approximation $\sigma = \sigma_2$ in the nonlinear term on the right hand side of Eq. 3.4. The general solution σ_1 of the resulting linearized equation is

$$\sigma_1 = \sigma_2\cos(\Omega y) + \dot{\sigma}_2\frac{\sin(\Omega y)}{\Omega} + \frac{S(\zeta)\left[e^{-y} - \cos(\Omega y) + \dfrac{\sin(\Omega y)}{\Omega}\right]}{\sigma_2(1+\Omega^2)}, \tag{3.5}$$

where $\dot{\sigma} \equiv d\sigma/dy$ and $\dot{\sigma}_2 = \sigma_2'\gamma_2/\gamma'$. Setting $\sigma_c = \sigma_1(y_c)$ and $\dot{\sigma}_c = \dot{\sigma}_1(y_c)$, we can perturbatively solve Eq. 3.4 in the second domain, assuming that the non-linear term on the

right hand side may be represented by a particular solution of the form given in Eq. 3.5.

The perturbative solution in the second region σ_{II} then becomes

$$\sigma_{II} = \left[\sigma_c - \frac{S(\zeta)e^{-y_c}}{\sigma_c \Psi}\right]\cos\left[\Omega_0(y-y_c)\right] + \frac{S(\zeta)e^{-y+(y_c-y)\dot{\sigma}_c/\sigma_c}}{\sigma_c\Psi} + \left[\dot{\sigma}_c + \frac{S(\zeta)e^{-y_c}(1+\dot{\sigma}_c/\sigma_c)}{\sigma_c\Psi}\right]\sin\left[\Omega_0(y-y_c)\right]/\Omega_0 \tag{3.6}$$

where $\Psi = \Omega_0^2 + (1+\dot{\sigma}_c/\sigma_c)^2$. The combination of Eqs. 3.5 and 3.6 , together with Eqs. A.1 and A.2, allows the description of the beam envelope from the initial conditions at the photocathode surface up to the photoinjector exit. While this treatment of the behavior of σ_{II} is quite general, it will ultimately prove less useful than one based on the invariant envelope given in the next section.

The whole system, *i.e.* the beam and the external RF and magnetic field, can be specified by means of ten operational quantities: the main quantities are the laser pulse characteristics (spot size at the cathode σ_r, pulse length $\sigma_z \equiv c\sigma_t$), the extracted bunch charge Q_b, the RF field quantities (field amplitude E_0 and RF frequency $\nu_{\rm rf}$), the magnetic field amplitude of the solenoid B_0, and the initial and final positions for the solenoid field distribution, namely z_b and z_c. The somewhat ancillary parameters associated with description of the RF field are η and μ (defined in Appendix A) which depend on the set of spatial harmonic coefficients a_n. In the following we will consider the special case of $\eta = \mu = 1$, *i.e.* a pure first harmonic RF field, because it greatly simplifies the analysis without significant loss of generality. In the following we take also $\phi = \pi/2$, which corresponds to the phase of maximum acceleration.

The beam envelopes resulting from this analysis applied to a multi-cell photoinjector are shown in Figs. 4 and 5, with several different values for B_0 for a typical set of photoinjector parameters (B_0 = 0 in Fig.4). In the upper diagram of Fig. 4 the bunch aspect

ratio is $A = 1.25$, with $\sigma_r = 1.5$ mm, corresponding to a peak current $I = 100$ A at $Q_b = 1$ nC ($I = Q_b c/\sqrt{2\pi}\,\sigma_z$) and 400 A at $Q_b = 4$ nC ($z_2 = 79$ mm, $\gamma_2 = 8.7$, $\alpha = 1.64$); in the lower diagram $A = 0.83$ with $\sigma_r = 2.0$ mm, giving $I = 200$ A at 4 nC ($z_2 = 174$ mm, $\gamma_2 = 8.6$, $\alpha = 1.62$). The simulations were performed with the codes ATRAP [12] for the S-band gun (Fig. 4 upper diagram) and ITACA [13] for the L-band case (Fig. 4 lower diagram). A similar comparison is shown in Fig. 5, where the extra focusing due to the magnetic field of solenoid is clearly displayed. It should be noted that by switching off the space charge term in Eqs. 3.5 and 3.6 one obtains the dotted curve plotted in Figure 5, for the case of $B_0 = 0.5$ kG, which is clearly mismatched with respect of the simulation curve, indicating the relevance of the non-linear space charge term in our analysis.

It is useful to recall that a transient angular kick $\Delta\sigma' = +\gamma'\sigma/2\gamma$ [6] (corresponding to $\Delta\dot{\sigma} = +\sigma/2$) must be added to the secular beam envelope at the gun exit in order to transform it back into the actual envelope. What is meant by the distinction *secular* in describing the envelope is the following: the secular envelope represents the actual envelope averaged over the cell-to-cell oscillations caused by the alternating gradient focusing effect associated with the backward component in the RF standing wave, as discussed in Ref. 6. The good agreement between the analytically predicted envelopes (dashed lines) and the numerical simulation data (solid lines) gives a significant confirmation on the capability of the present model to predict correctly, within the domain of interest, the beam envelope characteristics.

It is interesting to note that the first two terms on the right-hand side of Eq. 3.5, which scale linearly with the initial conditions σ_2 and $\dot{\sigma}_2$, correspond exactly to the linear transport matrix elements derived in Ref. 6 for the evolution of the secular envelope in RF linacs as far as $b = 0$, *i.e.* $\Omega = \Omega_0$ is set. Therefore, Equation 3.5 represents the extension of the analysis performed in Ref. 5 to the case of an external magnetic focusing added to the RF ponderomotive focusing, as well as the contribution from the space charge field, which is given by the third term on the right hand side of Eq. 3.5.

IV. THE CONCEPT OF INVARIANT ENVELOPE

Due to the excellent agreement between the analytical and numerical solutions to the envelope equation for space-charge dominated, strongly accelerating beams in the preceding section, we now extend our analysis to find a particular beam propagation mode. This mode will be shown to be analogous to the Brillouin flow for space charge dominated beams in focusing channels discussed in Section II.

First of all, we begin by transforming the envelope description in Eq. 3.4 from the Cauchy space (σ, y) into a dimensionless Cauchy (τ, y) space which displays the fundamental parametric dependence which governs the beam size evolution. By defining the dimensionless quantity $\tau \equiv \sigma / \sqrt{S}$ (we are now, for the sake of compactness, leaving as implicit the dependence of S on ζ), the envelope equation in the Cauchy dimensionless space (τ, y) reads

$$\frac{d^2\tau}{dy^2} + \Omega^2 \tau = \frac{e^{-y}}{\tau} \tag{4.1}$$

The scaling of the beam size with the square root of the perveance in this analysis naturally agrees with the scaling laws set down in Ref. 17, in that the beam plasma frequency is the same for any envelope of the same τ .

We are interested in the third region $(z > z_c)$, where, taking the case of $\eta = \mu = 1$ and $\phi = \pi/2$,which imply that $\Omega = \Omega_0 = 1/\sqrt{8}$, the envelope equation reads

$$\frac{d^2\tau}{dy^2} + \frac{\tau}{8} = \frac{e^{-y}}{\tau} \tag{4.2}$$

which is a universal scaled equation, independent of any external parameter.

Since the quantity $\sqrt{S}$ (which has units of a length) can be related to the transverse plasma frequency $\omega_p = \sqrt{\frac{4\pi n_e e^2}{\gamma^3 m_e}} = \frac{c}{\sigma}\sqrt{\frac{2I}{I_0\gamma^3}}$ by $\omega_p = \frac{c\gamma'}{\sigma\gamma}\sqrt{\frac{S\gamma_2}{\gamma}}$, it is interesting to note that the function τ can be expressed as $\tau = \frac{\gamma' e^{-y/2}}{\gamma k_p} = \frac{(\gamma'/\gamma)}{k_p}\sqrt{\frac{\gamma_2}{\gamma}}$ with $k_p = \omega_p / c$. In this form it is clearly shown that τ scales like the ratio between the local plasma wavelength $\lambda_p = 2\pi / k_p$, which sets the defocusing length of the beam, and the local incremental energy gain length $L_g = \gamma / \gamma'$, which sets both the beam adiabatic damping and RF focusing lengths.

Equation 4.2 has, like Eq. 3.4, a general perturbative solution,

$$\tau = \left[\tau_c - \frac{e^{-y_c}}{\tau_c \Xi}\right]\cos\left[\Omega_0(y-y_c)\right] + \frac{e^{-y+(y_c-y)\dot{\tau}_c/\tau_c}}{\tau_c\Xi} + \left[\dot{\tau}_c + \frac{e^{-y_c}(1+\dot{\tau}_c/\tau_c)}{\tau_c\Xi}\right]\sin\left[\Omega_0(y-y_c)\right]/\Omega_0 \quad , \tag{4.3}$$

with $\Xi = \frac{1}{8} + \left[1+\dot{\tau}_c/\tau_c\right]^2$ and $\Omega_0 = 1/\sqrt{8}$.

Within this family of solutions there is a notable particular solution,

$$\hat{\tau} = \sqrt{\frac{8}{3}}e^{-y/2} \quad , \tag{4.4}$$

corresponding to $\hat{\tau}_c = \sqrt{\frac{8}{3}}e^{-y_c/2}$, $\dot{\hat{\tau}}_c = -\sqrt{\frac{2}{3}}e^{-y_c/2}$, and $\Xi = \frac{3}{8}$. This solution is characterized by having a plasma frequency $\hat{k}_p = \sqrt{\frac{8}{3}}\frac{\gamma'}{\gamma}$ which is proportional to the ponderomotive RF focusing frequency and (imaginary) adiabatic damping frequency up to a fixed constant. Another way of viewing this is to note that the ratio between the two fundamental scale lengths, L_g and λ_p, is in this case exactly constant, *i.e.* $\hat{\lambda}_p / L_g = \sqrt{\frac{8}{3}}$.

This is achieved because the scaling of the plasma frequency as $\sqrt{n_b}\gamma^{-3/2}$ is exactly matched to the energy gain, including the reduction of the beam size $\hat{\sigma}$ with energy, which scales as $\gamma^{-1/2}$, namely $\hat{\sigma}=\frac{4}{\gamma'}\sqrt{\frac{I}{3I_0\gamma}}$. This constant relationship between L_g and λ_p also explicitly indicates that the invariant envelope is indeed an equilibrium-like solution in the Cauchy space. Further, it obviously displays the equilibrium-like that there are no periodic oscillations associated with it, but nearby orbits will oscillate about it; these oscillations will be studied in Section V.

The invariant envelope $\hat{\tau}$ has the extremely relevant property that it is the only solution displaying a constant phase space angle δ ($\delta \equiv \tau/\tau$), independent of initial conditions τ_c and $\dot{\tau}_c$ in all of the three spaces (Cauchy dimensionless (τ,y), Cauchy (σ,y), configuration space (σ,z)). In fact, $\hat{\delta}=\dot{\hat{\tau}}/\hat{\tau}=\dot{\hat{\sigma}}/\hat{\sigma}=-1/2$, so that in both Cauchy spaces the phase space angle is a universal constant, while in configuration space the phase space angle $\hat{\delta}_c \equiv \gamma\hat{\sigma}'/\hat{\sigma}=-\gamma'/2$ is a constant (the trace space angle is $\hat{\sigma}'/\hat{\sigma}=-\gamma'/2\gamma$).

Further, the most important attribute of $\hat{\delta}$ on the invariant envelope is that it does not depend on the beam current, which is embedded in the perveance scaled variables τ_c and $\dot{\tau}_c$. For this reason the solution $\hat{\tau}$ will be called the *invariant envelope*; its invariance in phase space angle with respect to current is exactly the basic condition to obtain a vanishing linear correlated emittance as the final state of the beam. In fact, it is well known that the emittance growth from linear space charge effects is due to the angular spread in phase space distribution of different bunch slices, which receive different kicks from the space charge field. In analogy to the discussion of the emittance oscillations in the beam mismatched to the solenoid in Section II, these different beam slices may be represented by different current amplitudes in Eq. 3.4, with the full beam represented by the ensemble of beam slices.

It is interesting to observe that, under the invariant envelope conditions, the space-charge term in Eq. 4.1, $\frac{e^{-y}}{\hat{\tau}} = \sqrt{\frac{3}{8}} e^{-y/2}$, is dominant over the focusing term, which is only one-third of the magnitude of the space-charge term, $\frac{\hat{\tau}}{8} = \frac{1}{3}\sqrt{\frac{3}{8}} e^{-y/2}$. Adiabatic damping of the angular divergence due to acceleration provides an additional (damping) term which counteracts the space-charge defocusing in the envelope equation, but it should be noted that the second derivative of the invariant envelope is always positive, thus classifying this trajectory as unstable. This in fact must be the case, since a stable trajectory would imply oscillatory, or nonlaminar, behavior: one of the main consequences of such a characteristic of the invariant envelope is the simultaneous damping of the beam spot size σ and the beam transverse momentum $p_\perp \equiv \gamma\hat{\sigma}' = -\gamma'\hat{\sigma}/2$ as $\gamma^{-1/2}$.

Since we solve the envelope equation under the assumption of laminarity, the range of validity of such an hypothesis should be investigated. Rewriting Eq. 4.1 by taking into account also the thermal emittance term defined by Eq. 2.2 we find

$$\frac{d^2\tau}{dy^2} + \Omega^2\tau = \frac{e^{-y}}{\tau} + \left(\frac{\varepsilon_{n,th}\gamma'\gamma_2 I_0}{2I}\right)^2 \frac{1}{\tau^3} \tag{4.5}$$

When the beam is on the invariant envelope $\tau = \hat{\tau}$, the second term on the right-hand side of Eq. 4.5 grows as $e^{3y/2}$, while the space charge term decreases as $e^{-y/2}$. In order to preserve the condition of quasi-laminarity, so that the beam can be considered space-charge dominated, the space charge term must be larger than the emittance term. This condition holds up to a position $y_l = \ln\left(\sqrt{\frac{8}{3}\frac{2I}{I_0\varepsilon_{n,th}\gamma'\gamma_2}}\right)$, beyond which the beam enters the region where becomes emittance dominated. This position corresponds to an energy γ_l given by

$$\gamma_l = \sqrt{\frac{8}{3}}\frac{2I}{I_0\varepsilon_{n,th}\gamma'}. \tag{4.6}$$

Since the thermal emittance $\varepsilon_{n,th}$ is typically of the order of 1 mm-mrad, and taking the relatively high accelerating gradient found in the plane-wave transformer (PWT) linac at UCLA, which is γ'=30 m^{-1} (E_0=30.6 MV/m), we have $\gamma_l = 6.4I[A]$. This energy is quite a bit larger than that obtained at the UCLA PWT (16 MeV), which like all existing standing wave photoinjectors has a peak energy less than 25 MeV, but with peak beam currents in excess of 50 A considered typical.

Another relevant assumption made above was that of longitudinal laminarity, which means that different slices do not mix with each other. This assumption is not violated in general since, as previously discussed, the longitudinal plasma period is much longer than the typical time scale of emittance compensation (*i.e.* of one plasma oscillation in the transverse plane). Since the longitudinal plasma frequency, which is suppressed in comparison to the transverse frequency by a geometrical factor $\omega_{p//} \cong \omega_{p\perp}\sqrt{g(\sigma_z)^{-1}-1}$, where for large beam rest frame aspect ratios $g \approx 1$, the number of plasma oscillations in the longitudinal plane is typically much smaller than one. The major result of this longitudinal plasma motion, which unlike the transverse motion has little restoring force, is to lengthen the pulse in a laminar fashion; there is relative motion of the beam slices, but they do not overtake each other.

When the beam leaves the accelerating structure one must add a positive (defocusing) kick $\Delta\sigma' = +\gamma'\sigma/2\gamma$, as previously mentioned, to obtain the correct connection between the secular envelope in the gun and the actual envelope outside. Since the corresponding kick in the Cauchy space is $\Delta\dot{\sigma} = +\sigma/2$, and in Cauchy dimensionless $\Delta\dot{\tau} = +\tau/2$, it can be clearly seen that a beam propagating through the structure on the invariant envelope, for which $\dot{\hat{\tau}} = -\hat{\tau}/2$, will exit the RF structure as a parallel beam, *i.e.* with $\dot{\tau} = \dot{\sigma} = \sigma' = 0$ and

$$\sigma_f = \frac{4}{\gamma'}\sqrt{\frac{I}{3I_0\gamma_f}}, \tag{4.7}$$

where γ_f is the exit beam energy. This condition is a useful experimental diagnostic of emittance compensation in practice.

The parallel exit condition on the beam envelope points out the analogy between the invariant envelope and the Brillouin flow. In fact the two flows can be matched at the exit of a standing wave linac; equating Eq. 4.7 with Eq. 2.2 one can find that a focusing gradient $K_r = \left(\sqrt{\frac{3}{8}}\frac{\gamma'}{\gamma_f}\right)^2$ produced by a solenoid of field amplitude $B_z = \sqrt{\frac{3}{2}}\frac{m_e c\gamma'}{e}$ can achieve this match, preserving the beam's mean angle in phase space to be vanishing after the linac.

The converse of the exit condition just discussed is the following entrance condition: a beam entering a standing wave linac must have initial beam size given by

$$\sigma_i = \frac{4}{\gamma'}\sqrt{\frac{I}{3I_0\gamma_i}}, \tag{4.8}$$

with vanishing divergence. In other words, the beam must also enter on a parallel trajectory. The implications of this condition for operation of a split photoinjector, consisting of a short RF gun followed by a drift space and a booster linac, are discussed in Section VI.

V. EMITTANCE COMPENSATION

External control of the beam spot size and emittance evolution in a long RF photoinjector is accomplished through the variation of the solenoid field strength, which allows one to launch, at $z = z_c$, a beam envelope which may be optimized for achieving low emittance performance. It is obvious from the previous section's discussion that this particular envelope solution is of interest from the point of view of emittance control, and so we now concern ourselves with two examination of two issues. The first is how to achieve this "matching" of the beam to the invariant envelope at the end of the solenoid, while the second is the investigation of the subsequent phase space dynamics of a real beam ensemble with a spread in trajectories. Both of these issues are critical in understanding the phenomenon of emittance compensation. We have argued that operation on the invariant envelope is the condition for optimum emittance compensation, in the sense that the beam (the ensemble of all beam slices) fully matched to the invariant envelope displays no further emittance oscillations. It will be shown below that this is only part of the story; beam slices which are not directly on the invariant envelope perform stable oscillations around the invariant envelope, leading to secular damping of the normalized emittance of the full beam ensemble.

At this point, we now wish to find here proper gun operating conditions, in terms of the six free parameters (spot size at the cathode σ_r, pulse length σ_z, bunch charge Q_b, RF field amplitude E_0 and frequency ν_{RF}, magnetic field amplitude B_0), able to achieve a beam matched at $z = z_c$ to the invariant envelope. In order to reduce the number of free parameters we need to specify the matching conditions in the Cauchy dimensionless space, we turn to a set of four free parameters, α, A, Λ.and b, defined by

$$\alpha \equiv \frac{eE_0}{2mc^2k},\ A \equiv \frac{\sigma_r}{\sigma_z},\ \Lambda \equiv \frac{I}{(\gamma'\sigma_r)^2},\ b \equiv \frac{cB_0}{E_0}. \tag{5.1}$$

These quantities are physically described as follows: α is the dimensionless amplitude of the RF vector potential, A the bunch aspect ratio, Λ the Cauchy current density and b the magnetic-to-RF focusing ratio. These tuning parameters are linked to the six previous free parameters by $k = 2\pi\nu_{RF}/c$, $\gamma' = eE_0/mc^2$, $I = Qc/\sqrt{2\pi}\sigma_z$, while the Cauchy current density Λ is given[14], in terms of the current density J by $\Lambda = \frac{2\pi J}{\gamma'^2}$ and is linked to the Cauchy perveance S by $\Lambda = 2I_0\gamma_2\frac{S}{\sigma_r^2}$. The merit of the set of four parameters given in Eq. 5.1 consists in the possibility of expressing the beam conditions τ_2 and $\dot{\tau}_2$ at the exit of the second cell ($z = z_2$) entirely in terms of these four, as reported in Appendix A, instead of the previously used six parameters.

The matching conditions at $z = z_c$ can be expressed as

$$\sqrt{\frac{8}{3}}e^{-y_c/2} = \tau_2\cos(\Omega y_c) + \dot{\tau}_2\sin(\Omega y_c)/\Omega + \frac{\left[e^{-y_c} - \cos(\Omega y_c) + \sin(\Omega y_c)/\Omega\right]}{\tau_2\left(1+\Omega^2\right)}$$

$$\sqrt{\frac{2}{3}}e^{-y_c/2} = \Omega\tau_2\sin(\Omega y_c) - \dot{\tau}_2\cos(\Omega y_c) + \frac{\left[e^{-y_c} - \Omega\sin(\Omega y_c) - \cos(\Omega y_c)\right]}{\tau_2\left(1+\Omega^2\right)} \qquad (5.2)$$

where $\tau_2 = \tau_2(\alpha, A, \Lambda, b)$ and $\dot{\tau}_2 = \dot{\tau}_2(\alpha, A, \Lambda, b)$ are given by Eq. A.1, while $y_c = \ln\left[(1+(5/2+1/4)\pi\alpha)/(1+3\pi\alpha/2)\right]$ and $\Omega^2 = \left(1/8 + b^2\right)$. The first two parameters are restricted by practical considerations to a limited range, that is $0.7 \le \alpha \le 3$ and $1/4 \le A \le 2$. Therefore, we solve the two expressions in Eq. 5.2 by expressing their roots as $\Lambda_s = \Lambda_s(\alpha, A)$ and $b_s = b_s(\alpha, A)$ which can be well approximated by the expressions

$$\Lambda_s[kA] = \left[\frac{\sqrt{235 - 266\alpha + 283A - 188\alpha A + 80A^2 - 5.3A^3} - 15.64 - 13.2A}{1.33 + 0.94A}\right]^2 \qquad (5.3)$$

and

$$b_s = 10^{-2}\left[\begin{array}{l} 5.7\alpha - 28.5 + \dfrac{77.8+4.8A}{\alpha^{1/4}} - 0.15\Lambda_s(\alpha,A) + \\ \sqrt{\Lambda_s(\alpha,A)}\left(\dfrac{5.7}{\alpha^{1/4}} - 0.84 + 0.28A\right) - 7.1A \end{array}\right]. \tag{5.4}$$

These quantities are plotted in Figs. 6 and 7 respectively, as functions of α at different values for A, *i.e.* A=2, 1, 1/2 and 1/4. In general, the Cauchy current density Λ_s increases with α up to a maximum $\alpha_{\max}$ beyond which Λ_s is no longer defined. The behavior of the values of b_s are plotted in Fig. 7, for the same values of A, up to each corresponding $\alpha_{\max}$.

The upper part of the operating diagram in Fig. 6, the region above the dotted line, is in fact forbidden, because in this region the bunch charge is in excess of the maximum which can be extracted from the cathode surface. This fundamental limitation, as predicted theoretically[15] and observed experimentally[16], sets the maximum achievable current density $J_{\max}$, according to the non-relativistic Child-Langmuir law, in the form $J_{\max}[A/cm^2] = 300\gamma'/\sigma_b[ps]$, valid for short bunches ($\sigma_b[ps] << 1180/\gamma'$). The condition can be cast in terms of $\Lambda_{\max}$ as

$$\Lambda_{\max}[kA] = \frac{324}{\alpha \cdot \sigma_\phi[^\circ \mathrm{rf}]}. \tag{5.5}$$

The dotted line plotted in Fig. 6 represents the limitation $\Lambda_{\max}$ for a typical bunch length of $\sigma_\phi = 2^\circ$. Clearly, the optimum operating points should be relatively far from the $\Lambda_{\max}$ line, because of the severe energy spread induced by the longitudinal space charge field at extraction from the cathode surface (if operating on the line, the photoelectrons in the bunch tail would actually see a vanishing accelerating field at the cathode surface due to the cancelling of RF field by the space charge one). Such a correlated energy spread, *i.e.* the dependence of energy on the phase or slice position in the bunch, produces chromatic aberrations in the transport through the solenoid

field and RF focusing channel, which can prevent the emittance correction process from proceeding correctly. An obvious cure is the use of off-crest acceleration to compensate the space-charge induced energy spread with an opposite effect from the RF field. In practice, this may imply operation far off-crest if the Cauchy current density approaches the limit given by Eq. 5.5.

It is interesting, for sake of illustration, to plot the current density J and cathode spot size σ_r corresponding to the line $\Lambda_s(\alpha, A=1)$, drawn in the Cauchy operating diagram of Fig. 6, once the RF frequency $\nu_{\rm rf} = 2\pi\omega$ has been fixed to some representative values, namely 650 MHz, 1.3 GHz, 2.856 GHz and 6 GHz, as shown in Fig. 8 and 9. As anticipated from the Cauchy operating diagram, each frequency has a definite window in the RF field amplitude in which operation of the injector in the space-charge compensation regime is possible: the dashed lines set the maximum current density limit corresponding to, for the upper line, a bunch length of 5 psec, and for the lower line of 10 psec. The cathode spot size σ_r, plotted in Fig. 9, corresponds to a bunch charge of 1 nC; it is given by the relation $\sigma_r = \sqrt[3]{\frac{c}{\sqrt{2\pi}}\frac{Q_b A}{\Lambda\gamma'^2}}$, showing the expected scaling as $Q_b^{1/3}$ as anticipated in Ref.17 .

In order to better illustrate the predictions of the operating diagram in Fig.6, we choose a point on the diagram, specifically one on the $A=1$ line at $\alpha = 1.3$, which corresponds to $\Lambda_s = 144$ kA. Choosing the RF frequency to be 1300 MHz (L-band) we obtain $E_0 = 36$ MV/m for the peak cathode field and $\sigma_r = 0.87$ mm for the cathode spot size and $\sigma_r = 1.36^\circ$ RF for the bunch length, once we choose the bunch charge Q_b to be 1 nC. The peak current comes out to be $I = 137$ A while $b_s = 0.85$ implies a magnetic field $B_0 = 1.02$ kG . The three representative currents, corresponding to three slices, are in this case (cfr. Appendix B Eqs. B9 and B10) $I = 137$, $I^+ = 163$ and $I^- = 97$. The numerical integration of the envelope equation are shown in Fig.10(a) (solid lines), where the case for $B_0 = 0$ (no solenoid focusing) is also plotted (dashed lines). The corresponding three slice emittance is shown in Fig.10(b): as predicted, the normalized emittance is actually corrected only for the case of a beam following the invariant envelope.

We now are in a position to discuss in more detail how the emittance correction process works when the injector is operated under the invariant envelope mode, *i.e.* it is set at the prescribed Λ_s and b_s for a chosen A. Let us rewrite Eq. 3.4 in the third region ($y > y_c$) by explicitly showing the dependence of the Cauchy perveance S and the ponderomotive focusing frequency Ω_0 on the slice position ζ in the bunch:

$$\left[\frac{d^2}{dy_\zeta^2} + \frac{1}{8\sin^2(\langle\phi\rangle - k\zeta)}\right]\sigma(y_\zeta,\zeta) = \frac{S(\zeta)}{\sigma(y_\zeta,\zeta)}e^{-y_\zeta} \tag{5.6}$$

where the Cauchy perveance now becomes $S(\zeta) = \frac{2Ig(\zeta)}{I_0\gamma_c(\zeta)\gamma'(\zeta)^2}$, the average accelerating gradient $\gamma'(\zeta) = \alpha k\sin(\langle\phi\rangle - k\zeta)$ (with $\langle\phi\rangle$ defined as the bunch average phase) and the initial normalized energy $\gamma_c(\zeta) = 1 + \frac{3\pi\alpha}{2}\sin(\langle\phi\rangle - k\zeta) + \alpha\cos(\langle\phi\rangle - k\zeta)$. As indicated by the subscript ζ in the independent variable y_ζ, Eq. 5.6 represents actually a family of equations, one for each slice located at a distance ζ from the bunch central slice, in the variable $y_\zeta \equiv \ln\left[\frac{\gamma(\zeta)}{\gamma_2(\zeta)}\right] = \ln\left[\frac{1 + \alpha\cdot kz\cdot\sin(\langle\phi\rangle - k\zeta) + \alpha\cos(\langle\phi\rangle - k\zeta)}{\gamma_2(\zeta)}\right]$. This family of equations can be transformed, in analogy to Eq. 4.2, to read

$$\left[\frac{d^2}{dy_\zeta^2} + \frac{1}{8\sin^2(\langle\phi\rangle - k\zeta)}\right]\tau(y_\zeta,\zeta) = \frac{e^{-y_\zeta}}{\tau(y_\zeta,\zeta)} \tag{5.7}$$

where $\tau(y_\zeta,\zeta) \equiv \frac{\sigma(y_\zeta,\zeta)}{\sqrt{S(\zeta)}}$. The invariant envelope then reads

$$\hat{\tau} = \frac{2e^{-y/2}}{\sqrt{1 + \frac{1}{2\sin^2(\langle\phi\rangle - k\zeta)}}}, \tag{5.8}$$

which in configuration space is simply

$$\sigma(z,\zeta)=\frac{2}{\gamma'(\zeta)}\sqrt{\frac{2Ig(\zeta)}{\gamma(\zeta)I_0\left[1+\frac{1}{2\sin^2(\langle\phi\rangle-k\zeta)}\right]}}. \tag{5.9}$$

As already discussed in Section IV, we know that the condition to have a vanishing correlated emittance growth is that the phase space angle of different slices are equal. In this respect, any effect which induces a correlation, *i.e.* a ζ-dependence, will produce an emittance increase through the spread of phase space angles of the different slices. The RF effects are basically chromatic, and their phase dependence is typically quite a bit weaker than the dependence of the effective perveance in $Ig(\zeta)$ in Eq. 5.8, since $\lambda >> \sigma_z$. We thus neglect the chromatic contributions to the dynamics, and concentrate on the charge dependent effects in which the longitudinal correlation of the transverse space-charge field gives the Cauchy perveance S a slice-dependence through the geometrical factor $g(\zeta)$. This condition makes the transformation from Cauchy space (σ,y) to the dimensionless Cauchy space (τ,y) dependent on ζ, an effect which is absent in continuous beams, as previously discussed in Section II and analyzed further in Ref. 7. In this spirit we also set the average phase of the bunch to $\pi/2$, which corresponds to maximum acceleration. We therefore write Eq. 5.9, under these approximations, as $\sigma(z,\zeta)\cong\frac{4}{\gamma'}\sqrt{\frac{Ig(\zeta)}{3\gamma I_0}}$. It obviously is straightforward to generalize the following analysis to include arbitrary accelerating phase.

Under the assumption of a monoenergetic bunched beam, the Cauchy transformation from z to y is again ζ-independent, and we now write $S=S(\zeta)=\frac{2I}{I_0\gamma_2\gamma'^2}g(\zeta)$. We have already shown that the invariant envelope is characterized by a phase space angle independent of the Cauchy perveance S, and hence on the current. We now demonstrate that this condition corresponds to a vanishing correlated emittance growth. Since we are dealing with transverse forces

which are linear in the radial coordinate, the transverse trace space distribution of the quasi-laminar beam (r,r') is represented by an ensemble of straight segments, one for each slice in the bunch, as depicted in schematically in Fig. 11. In this figure only two of these line segments are drawn, one for the central slice (located at $\zeta = 0$, having spot size σ_+ and divergence σ'_+), which is subject to the peak space charge field, another for a slice located at $\zeta = \sigma_z$ (with trace space variables σ_- and σ'_-), where the space charge field is smaller for typically encountered current distributions, and this reduction is represented by the geometrical factor $g(\sigma_z) < 1$. The normalized rms transverse emittance, defined by the relation $\varepsilon_n(z) \equiv \beta\gamma\varepsilon(z) \cong \gamma\varepsilon(z)$, with $\varepsilon(z)$ given in Eq. 2.7, is explicitly evaluated as

$$\begin{aligned} \varepsilon_n(z) &= \frac{\gamma}{2}\sqrt{\left(\sigma_+^2+\sigma_-^2\right)\left(\sigma_+'^2+\sigma_-'^2\right)-\left(\sigma'_+\sigma_+ + \sigma'_-\sigma_-\right)^2} \\ &= \frac{\gamma}{2}\sqrt{\left(\sigma_+\sigma'_- - \sigma_-\sigma'_+\right)^2} = \frac{\gamma}{2}\left|\sigma_+\sigma'_- - \sigma_-\sigma'_+\right| \end{aligned} \qquad (5.10)$$

As can be seen from Eq. 5.10, the rms emittance in this two-slice case is identical to the common geometrical definition of emittance; it is simply the area of the triangle given by the origin and the two rms phase space points corresponding to the slices.

It should be emphasized at this point that each slice is represented for simplicity by a straight segment in phase space, which is a zero emittance distribution, because we are neglecting the thermal emittance $\varepsilon_{n,th}$, according to our assumption of quasi-laminarity. In practice, this emittance, which is added in squares with spatially correlated sources of emittance, can be estimated to be $\varepsilon_{n,th} \approx \sigma_r\sqrt{kT/m_ec^2}$, where the effective (rest frame) temperature T of the beam electrons is determined by the photoemission process, which for metal photo-cathodes is less than 1 eV, and semiconductor cathodes is expected to be one order of magnitude smaller. With these thermal effects, each beam slice's phase space would be a bi-Gaussian distribution whose rms ellipse has an area (the *slice* emittance) proportional to the thermal emittance $\pi\varepsilon_{n,th}$. The emittance $\varepsilon_n(z)$ defined by Eq. 5.10 represents a reversible emittance growth which can be corrected by proper

beam manipulation, as we are discussing, while the thermal emittance $\varepsilon_{n,th}$ does not arise from reversible transformations and is, in this sense, a true Liouvillian invariant, as discussed in Ref. 15. It should also be recalled that we are neglecting the emittance due to nonlinear space-charge fields in this discussion as well.

Assuming for the sake of discussion that the two representative slices follow their own invariant envelopes, we have $\hat{\tau}_+ = \hat{\tau}_- = \hat{\tau} = \sqrt{\frac{8}{3}} e^{-\gamma/2}$, which implies $\sigma_+ = \frac{4}{\gamma'}\sqrt{\frac{I}{3I_0\gamma} g(\zeta = 0)}$ and $\sigma_- = \frac{4}{\gamma'}\sqrt{\frac{I}{3I_0\gamma} g(\zeta = \sigma_z)}$. For the invariant envelope, we have $\dot{\hat{\tau}}/\hat{\tau} = -1/2$, and thus $\sigma'_+ = -\frac{\gamma'}{2\gamma}\sigma_+$ and $\sigma'_- = -\frac{\gamma'}{2\gamma}\sigma_-$. It is readily verified that under these conditions that the normalized emittance defined by Eq. 5.10 vanishes; the invariant envelope is the propagation mode where all the bunch slices are aligned in the transverse phase space.

Clearly, to achieve this ideal beam propagation mode every slice in the bunch must be matched at the invariant envelope, that is $\sigma_c(\zeta)/\sqrt{S(\zeta)} = \hat{\tau}_c = \sqrt{\frac{8}{3}} e^{-\gamma_c/2} = \sqrt{\frac{8\gamma_2}{3\gamma_c}} \quad \forall \ \zeta$. This is an impossible condition to fulfil, and in practice, only a small section of beam can be exactly matched. In this regard, the matching discussed in previous Section, dealing with the conditions Λ_s and b_s necessary to operate the photoinjector on the invariant envelope, is clearly an rms matching, because the beam conditions τ_2 and $\dot{\tau}_2$ (Eqs. A.7 and A.8) are given in terms of the RF and space charge kicks averaged (in the rms sense) over the Gaussian charge distribution. Because of this, only a beam slice equivalent to rms beam is matched, the other beam slices can be considered in general to be mismatched from their invariant envelopes. The dynamics of these mismatched envelopes can be analyzed by perturbation of Eq. 5.6 or its equivalent about the invariant envelope of the matched slice. We thus assume in the following an rms matching and take the equivalent rms beam slice to be $\sigma_- = \hat{\sigma} = \hat{\tau}\sqrt{S_\sigma}$, with $S_\sigma \equiv S_{rms} \cong S(\zeta = \sigma_z)$, matched to the invariant envelope $\hat{\tau}$, while $\sigma_+ = (\hat{\tau} + \delta\tau)\sqrt{S_0}$ (with $S_0 \equiv S(\zeta = 0)$), is slightly mismatched by a quantity $\delta\tau$ from its invariant envelope.

Substituting σ_+ and σ_- in Eq. 5.10, and recalling that $\sigma' = \frac{\gamma'}{\gamma}\dot{\tau}\sqrt{S}$, we obtain

$$\varepsilon_n(z) = \frac{\gamma}{2}\left|(\sigma_- + \delta\sigma)\sigma_-' - \sigma_-(\sigma_-' + \delta\sigma')\right| = \frac{\gamma S_\sigma \hat{\tau}}{2}|\delta\tau + 2\delta\dot{\tau}|. \tag{5.11}$$

Expressing $\varepsilon_n(z)$ in terms of physical quantities associated with the invariant envelope, we find that

$$\varepsilon_n(z) \equiv \frac{2}{\gamma'}\sqrt{\frac{Ig(\sigma_z)}{3I_0\gamma}}|\delta\sigma\gamma' + 2\gamma\delta\sigma'| = \frac{\hat{\sigma}}{2}|\delta\sigma\gamma' + 2\gamma\delta\sigma'|, \tag{5.12}$$

where we set $g(0) = 1$. We can see that the normalized emittance is proportional to the beam size, which is monotonically decreasing on the invariant envelope; we shall now show that the term inside of the absolute value sign is in fact bounded, and so the emittance also displays a generally monotonically decreasing behavior.

We first study the behavior of deviations from the invariant envelope in Cauchy space, by linearize Eq. 5.6 around the solution represented by Eq. 5.7 to obtain, for the small amplitude motion about the invariant envelope

$$\delta\ddot{\tau} + \Omega^2\delta\tau - \frac{e^{-y}\delta\tau}{\hat{\tau}^2} = \delta\ddot{\tau} + \left(2\Omega^2 + \frac{1}{4}\right)\delta\tau = 0 \tag{5.13}$$

showing an oscillatory behavior

$$\begin{aligned}\delta\tau &= \delta\tau_c\cos[\omega(y-y_c)] + \frac{\delta\dot{\tau}_c}{\omega}\sin[\omega(y-y_c)] \\ \delta\dot{\tau} &= -\frac{\delta\tau_c}{\omega}\sin[\omega(y-y_c)] + \delta\dot{\tau}_c\cos[\omega(y-y_c)]\end{aligned} \tag{5.14}$$

for $\delta\tau$ around the invariant envelope with frequency $\omega = \sqrt{2\Omega^2 + 1/4}$, with the constants of integration derived from conditions at $y = y_c$. Since $\Omega^2 = (1/8)\sin^2\langle\phi\rangle = 1/8$, the motion around

the invariant envelope is stable, so that any beam injected slightly mismatched to the invariant envelope will follow a trajectory oscillating about it.

This stable motion has, like the small amplitude oscillations discussed in Section II, frequency independent of the space-charge strength. This is in fact a general property of the superposition of a linear focusing force with associated frequency Ω and a repulsive inverse power law force (power $-\alpha$) which has a particular equilibrium-like solution, in this case the invariant envelope. The small amplitude oscillations about this particular solution then have frequency $\sqrt{1+\alpha}\Omega$, which depends on the power exponent of the repulsive force, but *not* its strength, and is always proportional to the linear focusing force strength.

It can be seen in this case that the total potential must exhibits a local parabolic well at the intersection point of the attractive and repulsive force terms. The potential terms which give rise to these forces are shown by the Hamiltonian associated with Eq. 5.7,

$$H(y,\zeta)=\frac{p_\tau^2}{2}+\left[\frac{\tau}{4}\right]^2-e^{-y\zeta}\ln\tau\ ;\ p_\tau\equiv\dot{\tau}, \qquad (5.15)$$

in the conjugate variables (τ,p_τ). The Hamiltonian H is not a constant of the motion, as indicated by the explicit dependence on the independent variable y. The perturbed Hamiltonian, however, is a constant for small amplitude motion about the invariant envelope. The resultant simple-harmonic small amplitude motion can be seen to be manifestly Liouvillian, and the (τ,p_τ) phase space area (an emittance, which we discuss further below) is a constant of the motion as well. This fact guarantees that the normalized emittance must damp as $\gamma^{-1/2}$, as illustrated by the two-point emittance given by the second form of Eq. 5.11.

To further illustrate these points, it is perhaps more instructive to view the oscillations around the invariant envelope in physical variables at this point. The physical space analogue to Eq. 5.13 which describes oscillations about the invariant envelope can be written as

$$\delta\sigma'' + \left(\frac{\gamma'}{\gamma}\right)\delta\sigma' + \frac{1}{2}\left(\frac{\gamma'}{\gamma}\right)^2 \delta\sigma = 0. \tag{5.16}$$

This equation has the general solution

$$\begin{aligned} \delta\sigma &= \delta\sigma_c \cos(\psi) + \sqrt{2}\left(\frac{\gamma_c}{\gamma'}\right)\delta\sigma_c' \sin(\psi), \quad \text{with} \\ \delta\sigma' &= -\frac{1}{\sqrt{2}}\left(\frac{\gamma'}{\gamma}\right)\delta\sigma_c \sin(\psi) + \delta\sigma_c'\left(\frac{\gamma_c}{\gamma}\right)\cos(\psi), \end{aligned} \tag{5.17}$$

where $\psi \equiv \frac{1}{\sqrt{2}}\ln\left(\frac{\gamma}{\gamma_c}\right)$, $\delta\sigma_c = \sigma_c - \frac{4}{\gamma'}\sqrt{\frac{I}{3I_0\gamma_c}}$ and $\delta\sigma_c' = \sigma_c' + \sqrt{\frac{4I}{3I_0\gamma_c^{3/2}}}$ for the mismatched (core) envelope. It can be seen that the determinant of the matrix of the $(\delta\sigma, \delta\sigma')$ transformation is simply γ_c / γ, which is expected from adiabatic damping of the transverse oscillations. Thus we see that the *normalized offset emittance* associated with the phase space of the perturbed oscillations centred on the invariant envelope is conserved. This is to be expected from the Liouvillian nature of the perturbed envelope system.

Before discussing a general distribution, we first examine the behavior of the two-slice case introduced in Eqs. 5.9. In this case the emittance is given by

$$\varepsilon_n(z) \cong \frac{2}{\gamma'}\sqrt{\frac{Ig(\sigma_z)}{3I_0\gamma}}\left|(\delta\sigma_c\gamma' + 2\delta\sigma_c'\gamma_c)\cos(\psi) + (\delta\sigma_c'\gamma_c - \delta\sigma_c\gamma')\sqrt{2}\sin(\psi)\right|. \tag{5.18}$$

Equation 5.18 shows the expected $\gamma^{-1/2}$ damping of the normalized emittance, with anharmonic oscillations of periodicity 2 times shorter than the period of the perturbations about the invariant envelope.

For the case of a general n-slice distribution, with a symmetric spread in mismatch amplitude about the invariant envelope, it can be shown by extending the above arguments that the

normalized emittance that is projected by this distribution of phase space orbits offset from the origin in phase space, has the form

$$\begin{aligned}\varepsilon_n(z) &= \gamma\sqrt{\langle\delta\sigma^2\rangle\langle\delta\sigma'^2\rangle - \langle\delta\sigma\delta\sigma'\rangle^2 + \hat{\sigma}^2\left[\langle\delta\sigma'^2\rangle + \frac{\gamma'}{\gamma}\langle\delta\sigma\delta\sigma'\rangle + \left(\frac{\gamma'}{2\gamma}\right)^2\langle\delta\sigma^2\rangle\right]} \\ &= \sqrt{\varepsilon_{\text{off}}^2 + \hat{\sigma}^2\left[\langle(\gamma\delta\sigma')^2\rangle + \gamma'\langle\delta\sigma(\gamma\delta\sigma')\rangle + \left(\frac{\gamma'}{2}\right)^2\langle\delta\sigma^2\rangle\right]}\end{aligned}, \quad (5.19)$$

where we have defined used the definition of the normalized offset emittance of the distribution,

$$\varepsilon_{\text{off}} \equiv \gamma\sqrt{\langle\delta\sigma^2\rangle\langle\delta\sigma'^2\rangle - \langle\delta\sigma\delta\sigma'\rangle^2}, \quad (5.20)$$

and the indicated averages are over the n-slice distribution. The normalized offset emittance is a constant of the motion; it can be evaluated, for example, at the beginning of invariant envelope propagation as $\varepsilon_{\text{off}} \equiv \gamma\sqrt{\langle\delta\sigma_c^2\rangle\langle\delta\sigma_c'^2\rangle - \langle\delta\sigma_c\delta\sigma_c'\rangle^2}$. It is also clear from Eqs. 5.17 that the term inside the square brackets in Eq. 5.19 is bounded and oscillatory. Therefore we can write the general form of emittance evolution as

$$\varepsilon_n(z) = \sqrt{\varepsilon_{\text{off}}^2 + \hat{\sigma}^2\left(a + b\cos^2[\psi + \theta_c]\right)}, \quad (5.21)$$

where a, b and θ_c are constants describing the orientation of the offset distribution, and $\psi = 4k_p z/\sqrt{3}$.

A schematic picture of the phase space of a beam which is matched in the rms sense to the invariant envelope is shown in Fig. 12. For the sake of illustration, the familiar form of an ellipse is used to indicate the offset phase space distribution boundary. This ellipse has an invariant area $\pi\varepsilon_{\text{off}}$, and rotates with the same frequency as the envelope oscillations, $\omega = 4\omega_p/\sqrt{3}$. Fig. 12 shows the "secret" of emittance compensation; reassuringly, there is a Liouvillian space of orbits about the invariant envelope with conserved phase space area - the phase space-centred rms

emittance of beam damps as the offset from the origin $(\hat{\sigma},\hat{\sigma}')$ of the distribution approaches the origin in phase space. The normalized offset emittance can be therefore thought of as a strict lower bound on the phase space-centered normalized emittance of the distribution. One cannot actually extrapolate the damping of the emittance to this level, however, as this would violate the assumption of quasi-laminarity, which requires that the offset be larger than the spread of beam sizes in the distribution. This argument implies the normalized emittance must be several times larger than ε_{off}, when the emittance compensation process is halted by nonlaminar (cross-over) beam trajectories.

VI. THE CASE OF A COMPACT GUN WITH BOOSTER LINAC PHOTOINJECTOR

While the long RF photoinjector analyzed thus far is encountered in practice, with the noted examples of the LANL photoinjectors APEX and AFEL, it is much more common experimentally to employ a compact RF gun ($N+1/2$ cells, $N \leq 3$) followed by a drift space, and a booster linac. In this configuration, the beam is focused by a solenoidal field applied as it exits the short gun. The beam then drifts after focusing, undergoing a diminishing portion of an emittance oscillation as the beam becomes smaller, eventually minimizing as a beam waist is reached. The booster linac entrance is placed at this point to begin acceleration, extending further the process of emittance compensation. This waist should be chosen to both give a small emittance at the waist point and to match onto the invariant envelope associated with the beam current and energy, as well as the linac accelerating gradient. An illustrative example of such a system in shown in Fig. 13a, which displays the rms envelope and emittance evolution of the beam in the TTF-FEL photoinjector as obtained from a PIC simulation performed with ITACA [13]. The analytical prediction of the correct invariant envelope in this case is shown for comparison in Fig.13b. It is very close to this optimization found by performing many such simulations, thus validating the approach to photoinjector design we have deduced from this analysis.

The number N of full cells in the gun is variable in this analysis, but the validity of the approach followed here is confined to a few cells. The most commonly encountered case in practice, of course, is one full cell. We will also consider, as a particular case, the possibility to slightly vary the length of the first half cell, as it is known from experience that a slightly longer (typically 0.625 instead of 0.5) first cell gives better performances in terms of emittance correction. This generalization, while a departure from the model employed in the previous sections, is necessary for an accurate comparison of the theory to actual RF photoinjector configurations.

The basic strategy of the analysis presented in this section, in which we must specify the optimum envelope behavior in the drift space, is not a search for an invariant envelope-like

solution, but a matching of the beam envelope from the drift space to the invariant envelope of the booster linac. The model in this case is slightly changed with respect to that shown in Fig.3: first, the point z_c is now located at a variable position given by $z_c = [(1+d)/2 + N](\lambda/2)$, which becomes the end of the RF gun cavity structure, and the beginning of the drift section. Here the quantity d accounts for a change in the first half cell length, *i.e.* d=0.25 indicates a 25% lengthening (0.625 cell). We will also show that the optimum field profile for the solenoid magnetic is different from the previous (long gun) case, where the magnetic field begins at $z_{B1} = \lambda/8$ and ends at $z_{B2} = (5/4 + 1/8)\lambda$. For the compact injector the field start position is shifted downward at $z_{B1} = \lambda/2$, while the end position is shifted downward at $z_{B2} = (7/4)\lambda$. As discussed in the following, the longer magnetic field profile is needed basically to provide more focusing from the solenoid in a case where the ponderomotive RF focusing in the following cells is not only missing, but the exit defocusing transient kick at the end of the gun must be overcome.

The beam energy γ_c (at $z = z_c$) becomes $\gamma_c = \gamma_2 + (N-1)\pi\alpha$, with $\gamma_2 = \left[1 + \frac{3}{2}\pi\alpha\right]\left[1 + \frac{5}{12}d - \left(\frac{5}{2} + \frac{\pi^2}{3}\right)\frac{d^2}{24}\right]$ again the energy at the second iris position (as derived in Appendix A). Since the drift space downstream of z_c is free from any accelerating and/or focusing force, the envelope equation becomes, in this case,

$$\sigma'' - \frac{P}{\sigma} - \frac{\varepsilon_{n,th}^2}{\sigma^3 \gamma_c^2} = 0, \tag{6.1}$$

where $\sigma'' = \frac{d^2\sigma}{dz^2}$ and $P \equiv \frac{2I}{I_0 \gamma_c^3}$ is now defined as the beam perveance (the assumption γ_c>>1 is understood). According to the assumption of quasi-laminarity, we neglect the emittance term and cast Eq. 6.1 into the space (v, z) as

$$v'' - \frac{1}{v} = 0, \tag{6.2}$$

where $\nu(z) \equiv \sigma(z)/\sqrt{P}$. Typical values for the perveance are, in case of a 100 A beam at $\gamma_c = 1 + 5\pi/2 \cong 9$ $P \cong 1.6 \cdot 10^{-5}$, so that for a 1 mm beam spot size the quantity ν is of the order of 1, as is ν' when σ' is a few mrad. Eq. 6.2 can be derived from a Hamiltonian $H = \frac{p_\nu^2}{2} - \ln \nu$ $\left(\text{with } p_\nu \equiv \nu'\right)$, where H is now a constant of the motion, so that

$$\nu' = \sqrt{\nu_c'^2 + 2\ln\left(\nu/\nu_c\right)}, \tag{6.3}$$

which gives the trajectory solution for Eq. 6.2 in integral form

$$\int_1^{\nu/\nu_c} \frac{dx}{\sqrt{\nu_c'^2 + 2\ln x}} = \frac{(z - z_c)}{\nu_c}. \tag{6.4}$$

The integral in Eq. 6.4 is not analytically solvable unless the approximation $\left|1 - \nu/\nu_c\right| << 1$ is done, which is in fact typical of an RF gun operated in the emittance compensation regime, as the beam size oscillations must be kept small both to prevent nonlaminar trajectories and to keep the oscillation frequency nearly independent of the perveance. Indeed, in practice, the beam exits the gun with a small negative divergence σ_c', so that it is transported up to a space charge-dominated waist with a spot size usually slightly smaller than σ_c. In this case the approximate solution is

$$\nu(z) = \nu_c \left\{ 2 - \left| \frac{\nu_c - \nu_c' \Delta z}{\nu_c \nu_c' + \Delta z} \right| \sqrt{\left(1 + \nu_c'^2\right) \Big/ \left[1 + \left(\frac{\nu_c - \nu_c' \Delta z}{\nu_c \nu_c' + \Delta z} \right)^2 \right]} \right\} \tag{6.5}$$

where $\Delta z = z - z_c$. The initial conditions $\left(\nu_c, \nu_c'\right)$ are given, in terms of the beam conditions at the gun exit $\left(\tau_c, \dot{\tau}_c\right)$, by

$$\nu_c = \frac{\tau_c}{\gamma'} \sqrt{\frac{\gamma_c^3}{\gamma_2}} \quad , \quad \nu_c' = \left(\dot{\tau}_c + \frac{\tau_c}{2} \right) \sqrt{\frac{\gamma_c}{\gamma_2}}, \tag{6.6}$$

recalling that (ν_c, ν_c') correspond to actual envelope variables, which Eq. 6.6 connects to $(\tau_c, \dot{\tau}_c)$, secular envelope variables.

In order to match to the invariant envelope at the entrance of the booster linac, we need to find, the conditions under which the phase space angle corresponding to the solution to Eq. 6.2 is invariant with respect to the beam current I, or, equivalently, to the perveance P. This is equivalent to requiring

$$\frac{d(\sigma'/\sigma)}{dP} = \frac{d(\nu'/\nu)}{dP} = \frac{1}{\nu^2}\left(\nu\frac{d\nu'}{dP} - \nu'\frac{d\nu}{dP}\right) = 0. \tag{6.7}$$

Since $\frac{d\nu'}{dP} = \frac{1}{\nu'\nu}\frac{d\nu}{dP}$ (see Eq.6.3), we have $\frac{d(\nu'/\nu)}{dP} = \frac{1}{\nu'\nu^2}(1-\nu'^2)\frac{d\nu}{dP}$. Therefore, $\frac{d(\sigma'/\sigma)}{dP} = 0$ if either $\nu'^2 = 1 \ \forall \ z$ (which is not possible to fulfil, because it is not a solution of Eq. 6.2) or $\frac{d\nu}{dP} = 0$. Since ν depends on P through the initial conditions (ν_c, ν_c'), the condition $\frac{d\nu}{dP} = 0$ is equivalent to

$$\frac{d\nu_c}{dP} = \frac{d\nu_c'}{dP} = 0, \tag{6.8a}$$

which in turns is equivalent to the condition

$$\begin{cases} \frac{d\tau_c}{d\Lambda} = 0 \\ \frac{d\dot{\tau}_c}{d\Lambda} = 0 \end{cases}, \tag{6.8b}$$

where the Cauchy current density is given by $\Lambda = \frac{I}{(\gamma'\sigma_r)^2}$.

It should be noted, however, that the invariance of the phase space angle at the end of the drift given by Eq. 6.7 is achieved only through the invariance of the initial conditions versus the current. The reason for this is that the phase space angle ν' / ν associated with Eq. 6.5 is not intrinsically invariant, unlike the case of the invariant envelope, where the phase space angle is a constant $\dot{\tilde{\tau}} / \tilde{\tau} = -1/2$. In this respect, Eq. 6.2 does not display any invariant envelope solution, *i.e.* any solution for which $\nu' / \nu = const.$ equivalent to the Brillouin flow condition given in Eq. 2.2, where the phase space angle is again a constant $\sigma'_{eq} / \sigma_{eq} = 0$.

To better clarify this point let us examine the equation for small deviations $\delta\nu$ around an equilibrium solution ν_0 of Eq. 6.2. Assuming $\delta\nu / \nu_0 << 1$, we find

$$\delta\nu'' + \frac{\delta\nu}{\nu_0^2} = 0, \tag{6.9}$$

giving stable oscillations with frequency $1/\nu_0$ around the equilibrium solution ν_0. As far as the beam envelope can be represented by the approximate solution (Eq. 6.5) in the drift space, implying that the beam size varies slightly between the initial condition ν_c and the beam spot at the waist ν_w, we may identify ν_0 roughly with the expression of Eq. 6.5, so that the drift space up to the waist (and slightly further away) is comparable to a quasi-Brillouin flow condition with a *local* stability condition similar to the one described in Section II. Since the beam size, in absence of any focusing, grows indefinitely after the waist, the frequency of oscillation $1/\nu_0$ around the equilibrium solution is decreasing and the nonlinearities (see Eq. 2.7) in the oscillations preclude any further vanishing point in the correlated emittance, as clearly illustrated in examples shown below.

It is interesting to notice that Eqs. 6.8 are equivalent to a vanishing correlated emittance at the *waist* position; this requires that the waist position $\Delta z \equiv z_w - z_c$ and the waist beam spot size ν_w are independent of the perveance,

$$\begin{cases} \dfrac{d\Delta z_w}{dP} = 0 \\ \dfrac{dv_w}{dP} = 0 \end{cases} \quad \text{with} \quad \begin{cases} \Delta z_w = v_c f(v_c') \;\; ; \;\; f(v_c') \equiv \displaystyle\int_{e^{-v_c'^2/2}}^{1} \frac{dx}{\sqrt{v_c'^2 + 2\ln x}} . \\ v_w = v_c e^{-v_c'^2/2} \end{cases} \tag{6.10}$$

The function $f(v_c')$ is plotted versus v_c' in Figure 14. For the purpose of further analysis, we note that $f(v_c')$ can be approximated (within a 5% error) by the function $g(v_c') = \dfrac{1.09\, v_c'}{1.69 + v_c'^2} + 0.423\, v_c' e^{-0.296 v_c'^2}$, in the range $|v_c'| \le 6$. This range easily covers all RF photoinjectors of interest, as a larger value of $|v_c'|$ implies a strongly convergent beam which will be susceptible to nonlaminar behavior near the waist. The conditions in Eq. 6.10 are now written explicitly in terms of the initial conditions at the start of the drift as

$$\begin{cases} f(v_c')\dfrac{dv_c}{dP} + v_c \dfrac{df(v_c')}{dv_c'}\dfrac{dv_c'}{dP} = 0 \\ \dfrac{dv_c}{dP} - v_c v_c' \dfrac{dv_c'}{dP} = 0 \end{cases} . \tag{6.11}$$

This system of equations allows solutions different from $\dfrac{dv_c}{dP} = \dfrac{dv_c'}{dP} = 0$ if the determinant of the coefficient matrix, $\det M = -v_c \left[v_c' f(v_c') + \dfrac{df(v_c')}{dv_c'} \right]$, is vanishing. By applying the Leibniz formula for the derivation of definite integrals, we find $\dfrac{df(v_c')}{dv_c'} = 1 - v_c' f(v_c')$, so that $\det M = -v_c$, which can never be vanishing, implying that the conditions $\dfrac{dv_c}{dP} = \dfrac{dv_c'}{dP} = 0$ and $\left[\dfrac{d\Delta z_w}{dP} = 0 \;;\; \dfrac{dv_w}{dP} = 0 \right]$ are in fact equivalent.

In order to derive the solution to Eq. 6.8 in terms of the beam conditions $(\tau_2, \dot{\tau}_2)$ at the second iris position $(z = z_2)$, as reported in Appendix A, we approximate the envelope equation in the region of drift with applied solenoid field (*i.e.* $z_2 < z < z_{B2}$) as

$$v'' + K_r v = \frac{1}{v_2} \tag{6.12}$$

where $\nu_2 \equiv \frac{\sigma_2}{\sqrt{2I/(I_0\gamma_2^3)}}$, and $K_r = \left(\frac{b\gamma'}{\gamma_2}\right)^2$, and so the space charge term is taken as a constant, its the value assumed at the gun exit. This is valid only for a 1+1/2 cell gun, for which the beam energy at the exit, γ_2, is constant all over the drift space: however, the treatment can be easily generalized to the case of a N+1/2 cell gun. In the N=1 the drift space is divided into two parts. In the first one, from $z = z_2 = (3/4)\lambda$ up to $z = z_c = z_{B2} = (7/4)\lambda$, the beam is subject to a focusing solenoid field, while for $z > z_c$ the drift is in free space. Under this approximation Eq. 6.12 can be easily solved to find

$$\begin{cases} \nu_c = \nu_2 \cos\theta + \dfrac{(1-\cos\theta)}{\nu_2 K_r} + \nu_2' \dfrac{\sin\theta}{\sqrt{K_r}} \\ \nu_c' = -\nu_2 \sqrt{K_r} \sin\theta + \dfrac{\sin\theta}{\nu_2 \sqrt{K_r}} + \nu_2' \cos\theta \end{cases} \tag{6.13}$$

where $\theta = \sqrt{K_r}(z - z_2)$, and hence

$$\begin{cases} \dfrac{d\nu_c}{dP} = \dfrac{d\nu_2}{dP}\left[\cos\theta - \dfrac{(1-\cos\theta)}{\nu_2^2 K_r}\right] + \dfrac{d\nu_2'}{dP}\dfrac{\sin\theta}{\sqrt{K_r}} \\ \dfrac{d\nu_c'}{dP} = \dfrac{d\nu_2}{dP}\left[-\sqrt{K_r}\sin\theta - \dfrac{\sin\theta}{\nu_2^2\sqrt{K_r}}\right] + \dfrac{d\nu_2'}{dP}\cos\theta \end{cases} \tag{6.14}$$

The determinant of the coefficient matrix is derived to be $\det M_2 = 1 + \frac{1-\cos\theta}{\nu_2^2 K_r}$, which clearly implies $\det M_2 > 1$, indicating that the only solution is $\frac{d\nu_2}{dP} = \frac{d\nu_2'}{dP} = 0$, which we know to be equivalent to

$$\begin{cases} \dfrac{d\tau_2}{d\Lambda} = 0 \\ \dfrac{d\dot{\tau}_2}{d\Lambda} = 0 \end{cases} \tag{6.15}$$

where τ_2 and $\dot{\tau}_2$ are specified in Eqs. A.7 and A.8 as functions of (α, A, Λ, b). Following the same procedure as in Section V, we solve these two equations by expressing their roots as $\Lambda = \Lambda(\alpha, A)$ and $b = b(\alpha, A)$. The system is highly non-linear, so that we start by expressing the first of Eqs. 6.14 as

$$\frac{d\tau_2}{d\Lambda} = \frac{1}{\Lambda}\left\{\sqrt{\frac{\Lambda\gamma_2}{2I_0}}\frac{\pi\zeta(A)}{4}\left[1-\frac{\ln\gamma_2}{\gamma_2-1}\right]-\tau_2/2\right\}=0 \qquad (6.16)$$

which can be solved for the variable $b = \sqrt{2}\sqrt{1+\left(1-\frac{\pi\zeta(A)\Lambda}{4I_0}\right)\left[1-\frac{\ln\gamma_2}{\gamma_2-1}\right]}\Big/\ln\left(\frac{\gamma_2}{\gamma_b}\right)$.

Substituting back into the second of Eqs 6.15, we obtain an equation in Λ, α and A. By a fitting procedure we obtain the following solutions

$$\Lambda^{opt}\ [kA] = 57.3 - 12.4\alpha + 2.63\alpha^2 + 26.2A - 1.78\alpha A + 1.86A^2 \qquad (6.17)$$

and

$$b^{opt} = 1.49 + \frac{1.67}{\sqrt{\alpha}} - \frac{2.07}{\alpha^{1/4}} \qquad (6.18)$$

The Cauchy perveance Λ^{opt} is plotted in Fig. 15 (solid lines) as a function of α for some usual values of A. It is interesting to note that Λ^{opt} is nearly independent of α for $\alpha \geq 1.5$, while it decreases almost linearly with α for $\alpha \leq 1.5$. Its dependence on A is fairly linear in most of the diagram, so that the following scaling laws hold:

$$\begin{aligned} \Lambda^{opt} &\propto A \ \text{ if } \ \alpha \geq 1.5 \\ \Lambda^{opt} &\propto A(3-\alpha) \ \text{ if } \ \alpha \leq 1.5 \end{aligned} \qquad (6.19)$$

which can be cast in terms of the bunch charge Q_b, cathode spot size σ_r, accelerating gradient γ' and RF wave number k

$$\begin{aligned} Q_b &\propto \sigma_r^3 \gamma'^2 \quad \text{if } \alpha \geq 1.5 \\ Q_b &\propto \sigma_r^3 \gamma'^2 (3 - \gamma'/k) \quad \text{if } \alpha \leq 1.5 \end{aligned} \tag{6.20}$$

which resemble the scaling laws reported in Ref. 17.

As in Fig.6, the Cauchy perveance $\Lambda_{\max}$ (see Eq. 5.4) compatible with the maximum charge limit is plotted in Fig.15 (dotted lines) for a bunch length $\sigma_\phi = 2^\circ$ (the higher line) and $\sigma_\phi = 4^\circ$ (the lower line).

The parameter b^{opt}, which represents the ratio between magnetic and RF focusing, turns out to be nearly independent or the aspect ratio A, as shown in Fig.16, where b^{opt} is plotted as a function of α for different values of A (it should be noted that Eq. 6.18 displays a simplified form for b^{opt} which has already removed the very weak dependence on A). It should be also noted that b^{opt} is much higher than the analogous parameter b_s (see Fig.7) required in the case of the indefinitely long photoinjector. This is due to the fact that the additional RF focusing applied in the long photoinjector is missing here, causing the need of an enhanced extra-focusing from the external solenoid.

The current density J corresponding to the Λ_s lines is plotted (solid lines) in Fig. 17, for some selected RF frequencies (650 MHz, 1.3, 3 and 6 GHz), at aspect ratio $A = 1$. The maximum limits for the current density are also reported, in case of $\sigma_t = 5$ psec (higher dashed line) and $\sigma_t = 10$ psec (lower dashed line). The required cathode spot size σ_r (for the case of a 1 nC bunch charge) are plotted in Fig.18, for the same set of frequencies and at different bunch aspect ratios.

It should be noted that the operating point to achieve the emittance compensation shown in Fig.13a and 13b has been derived by the operating diagram in Fig.15, selecting the point $\alpha = 1.8$, $A = 1/2$, $\Lambda = 56$ kA, giving at L-band $E_0 = 50$ MV/m, $\sigma_r = 0.76$ mm and

$$\sigma_w^{opt}[\mathrm{mm}] = \frac{\sqrt{I[A]}}{\gamma'[m^{-1}]}\left[\begin{array}{l} 3.76 + 1.56\alpha - 1.58\alpha^2 + 0.26\alpha^3 + 0.56A + \\ 0.914\alpha A - 0.11\alpha^2 A - 0.15\alpha A^2 \end{array}\right]. \qquad (6.23)$$

As an example, for an L-band injector operated at $\nu_{RF} = 1.3\ GHz$, with $E_0 = 56$ MV/m ($\gamma' = 55\ \mathrm{m}^{-1}$, and $\alpha = 2$) the optimum Λ at $A = 1$ will be $\Lambda^{opt} = 68$ kA, while $b^{opt} = 0.92$, so that the solenoid field will be B_0=1.7 kG. Assuming a bunch charge $Q_b = 1$ nC, the laser spot size at the cathode σ_r will be, recalling that $\sigma_r = \sqrt[3]{\frac{c}{\sqrt{2\pi}}\frac{Q_b A}{\Lambda\gamma'^2}}$, $\sigma_r = 0.84$ mm. The beam current will be given by $I = \frac{Q_b c}{\sqrt{2\pi}\sigma_z} = \frac{Q_b c A}{\sqrt{2\pi}\sigma_r} = 142$ A, so that the beam spot size at the waist will be $\sigma_w^{opt} = 0.94$ mm, while at the gun exit $\sigma_2 = 1.9$ mm. The waist will be located at $z_w^{opt} = 0.793$ m. It is remarkable to note that the waist position scales with explicit dependence only on the RF field and wavelength, not the bunch charge and/or current (which are derived quantities), in agreement to what is observed in Ref. 17.

In case the first half cell is lengthened by, say, twenty percent, as is done in many new RF gun designs, we have re-calculated Λ^{opt} and b^{opt}, to obtain

$$\Lambda^{opt}\ [kA] = 58.33 - 11.83\alpha + 2.52\alpha^2 + 27.34A - 1.816\alpha A + 1.88A^2, \quad \text{and} \qquad (6.24\text{-a})$$

$$b^{opt} = 1.38 + \frac{1.52}{\sqrt{\alpha}} - \frac{1.86}{\alpha^{1/4}}, \qquad (6.24\text{-b})$$

i.e. behavior very close to that one of the standard half cell. The predicted position and spot of the waist now become

$$z_w^{opt} = (\frac{7}{4})\lambda + \frac{1}{\gamma'}\left[9.94\alpha + 2.59\alpha^2 + 0.18A - 2.65\alpha A - 2.96\right] \qquad (6.25)$$

$$\sigma_w^{opt}[\mathrm{mm}] = \frac{\sqrt{I[\mathrm{A}]}}{\gamma'[\mathrm{m}^{-1}]}\left[\begin{array}{l} 5.2 + 2.14\alpha - 1.77\alpha^2 + 0.27\alpha^3 + 0.19A + \\ 0.95\alpha A - 0.058\alpha^2 A - 0.19\alpha A^2 \end{array}\right] \qquad (6.26)$$

Taking the same example as before, i.e. for an injector operated at L-Band ($\nu_{RF} = 1.3\ GHz$) and $E_0 = 55.7\ MV/m$ (hence $\gamma' = 54.6\ m^{-1}$ and $\alpha = 2$) the optimum Λ, at $A = 1$, is now $\Lambda^{opt} = 70.4\ kA$, while $b^{opt} = 0.89$, so that the solenoid field will be B_0=1.64 kG. With a bunch charge $Q_b = 1\ nC$, the laser spot size at the cathode σ_r is now $\sigma_r = 0.83\ mm$, and the beam current becomes $I = 144\ A$, so that the main parameters are almost unchanged, as for the waist position, which is $z_w^{opt} = 0.804\ m$. On the opposite, the beam spot size at the waist is now larger, being $\sigma_w^{opt} = 1.3\ mm$.

VII. CONCLUSIONS

We have discussed, in some detail, the properties of the invariant envelope, which is a particular beam propagation mode characterized by a phase space angle which is a globally constant. Under the hypothesis of quasi-laminarity, which is equivalent to the assumption that the beam is space charge dominated and the number of plasma oscillations considered are small (in order to avoid transverse and longitudinal mixing), we have shown that the invariant envelope is a mode propagation which damps the correlated emittance - provides emittance compensation - as $1/\sqrt{\gamma}$, so that the possible emittance dilution of a beam, due to longitudinal-transverse correlations caused by either space charge or any other source (RF, etc.), can be corrected by transporting the beam under an invariant envelope mode. While we have concentrated here on standing wave linacs, the invariant envelope exists in other types of structures, with and without externally applied focusing forces, as summarized in Table I. In general, RF linacs allow acceleration under invariant envelope both in standing and travelling wave operation where the correlated emittance oscillations are damped due to acceleration as the invariant envelope beam spot scales like $1/\sqrt{\gamma}$. Drift spaces, on the other hand can be operated in the invariant envelope only with an external focusing to set up a true Brillouin flow condition: the drift space after a compact photoinjector is, in this respect, only an approximation of invariant envelope.

Also, this In any case, the emittance oscillations are not damped in drifts, so that one must quickly accelerate the beam after the drift, starting from the first emittance minimum, if the onset of thermalizing processes, which transform the reversible emittance oscillation into an irreversible temperature emittance growth, are to be avoided.

Beam Transport	Invariant envelope	Space	Emittance damping
Standing wave linac	Secular $\frac{2e^{-y/2}}{\sqrt{\frac{\eta}{2\sin^2<\phi>}+1}}$	Cauchy dimensionless	Yes
Standing wave linac plus solenoid	Secular $\frac{e^{-y/2}}{\sqrt{\frac{\left(\frac{\eta}{8}+b^2\right)}{\sin^2<\phi>}+\frac{1}{4}}}$	Cauchy dimensionless	Yes
Travelling wave linac	Actual $2e^{-y/2}$	Cauchy dimensionless	Yes
Travelling wave linac plus solenoid	Actual $\frac{e^{-y/2}}{\sqrt{\frac{b^2}{\sin^2<\phi>}+\frac{1}{4}}}$	Cauchy dimensionless	Yes
Drift	No	Real dimensionless	No
Drift plus solenoid	Brillouin Flow $\sigma_{eq}=\sqrt{\frac{P}{K_r}}$	Real dimensionless	No

Table I. Properties of invariant envelope flow, where possible, in various types of beam transport and acceleration.

As shown in the table, travelling wave linacs operated with an extra magnetic focusing, provided by a solenoid surrounding the accelerating section, may be in principle equivalent to standing linacs, where the focusing is provided by the RF ponderomotive effect, as long as the magnetic focusing ratio $b \equiv cB_0/E_0$ is chosen to have the value $b=\sqrt{\eta/2}$.

A transport line made by different sections which are all operated under their own invariant envelope mode is of course a global invariant envelope beam propagation. The

final design of a photoinjector which must be operated in the emittance correction regime will be therefore made up by a *Lego"* -like array of accelerating and drift sections properly matched and operated under invariant envelope. Care must be taken that this array include the final transport from the booster linac to the application, so as to avoid emittance growth after initial compensation. In general this means, for transport which is longer than one-quarter of a plasma wavelength, that the beam be focused often enough (typically by quadrupoles) to approximate Brillouin flow after the photoinjector linac, with the beam controlled so as to not make large excursions in spot size. For discrete focusing elements such as quadrupoles, this means that the elements must be placed within one-quarter of a plasma wavelength of each other.

In matching different sections one should however be careful about what kind of orbit the invariant envelope is expressed to: *secular* or actual. In standing wave linacs the envelope is given in terms of a secular orbit, i.e. an orbit averaged over the cell-to-cell oscillations, so that at the entrance of the structure one must subtract a focusing $\Delta\sigma' = -\gamma'\sigma / 2\gamma$ kick to the beam envelope conditions of the previous section in order to match to the secular envelope. In case the previous section is the drift space between short RF gun and a booster linac, one should position the space charge dominated waist directly at the entrance of the linac, as discussed in Section VI: the initial divergence of the secular envelope in the booster will be in this way $\sigma' = -\gamma'\sigma / 2\gamma$, which is exactly the first condition to be on the invariant envelope. The second condition, i.e. $\sigma = \frac{4}{\gamma'}\sqrt{\frac{I}{3I_0\gamma}}$, can be easily achieved by simply tuning the accelerating gradient γ' for a given energy, current and spot size of the beam at the booster entrance. It is remarkable to note that this prescription on the matching condition has been observed in several simulations of RF photoinjectors[18].

If the booster linac is a travelling wave structure the matching conditions are different because the envelope is expressed in terms of the actual orbit and no transient kick

must be applied at the booster entrance. A converging beam should be injected into the booster, in this case, in order to match the invariant envelope conditions: this is again in agreement with the results of multiparticle simulations[19].

Finally, in case of a long multi-cell RF photoinjector structure we recall that the beam, if transported under the invariant envelope, must leave the photoinjector cavity with zero divergence. Due to the typical high energy of the beam, as in case of the 10+1/2 cell AFEL photoinjector [20], the beam envelope is assumed to stay parallel for a long drift after leaving the photoinjector[21]. Therefore, a parallel matched beam emerging from a long multi-cell photoinjector is therefore a sign of proper operation in the emittance compensation regime, as experimentally observed[22].

REFERENCES

1. J.S. Fraser, *et al., IEEE Trans. Nucl. Sci.* **NS-32**, 1791 (1985).
2. C. Travier, *Particle Accelerators* **36**, 33 (1991).
3. X. Wang, submitted to *Physical Review Letters.*
4. B.E. Carlsten, *Nucl. Instr. Methods A* **285**, 313 (1989).
5. J.D.Lawson, *The Physics of Charged Particle Beams*, 2nd Ed. (Oxford University Press, New York, 1988).
6. J.B.Rosenzweig and L.Serafini, Phys. Rev. E **49**, 1599(1994); S.C. Hartman and J.B.Rosenzweig, Phys. Rev. E **47**, 2031 (1993).
7. L.Serafini, *Particle Accelerators* **49**, 253 (1995).
8. P. Lapostolle, *Proton Linear Accelerators* (Los Alamos, 1980).
9. K.J. Kim, *Nucl. Instr. Methods A* **275**, 201 (1989).
10. J. Coacolo, private communication.
11. L.Serafini, R.Zhang and C.Pellegrini, in publ. on *Nucl. Instr. Methods A.* (1996).
12. J.M. Dolique and J.C. Coacolo, *Nucl. Instr. Methods A* **340**, 231 (1994).
13. L.Serafini, C.Pagani, *Proc. Eur. Particle Accel. Conf.* 866 (1988,World Scientific).
14. The current density J is not the real beam current density along acceleration: it is just a reference value calculated with the beam spot size at the cathode σ_r.
15. C. Travier, Ph.D. Thesis, Universite' De Paris Sud, Orsay-LAL, Dec. 15th 1995.
16. J.B. Rosenzweig, *et al., Nucl. Instr. Methods A* **341**, 379 (1994).
17. J.B. Rosenzweig and E. Colby, in *Advanced Accelerator Concepts*, **335**, 724 (American Inst. Physics, 1995).
18. E. Colby, J.-F. Ostiguy, and J.B. Rosenzweig, in *Advanced Accelerator Concepts* **335**, 708 (American Inst. Physics,, 1995).
19. D.T. Palmer, *et al.* in *Proc. 1995 IEEE Particle Accel. Conf.* 2432 (IEEE, 1996).
20. D.C. Nguyen et al., *Nucl. Instr. Methods A* **341**, 29 (1994).
21. Taking indeed a 100 A beam at 19 MeV, the beam spot at the photoinjector exit, as predicted by the invariant envelope mode, is $\sigma = 0.9\ mm$, so that Eq. 6.1 predicts a spot size increase of less than 125 μm over 1 m drift.
22. R. Sheffield, private communication.

APPENDIX A

The expressions for the beam exit conditions σ_2 and σ_2' at the second iris location $z = z_2$ are reported in this Appendix. The expressions given have been derived for a Gaussian charge distribution in the bunch, of dimensions σ_r and σ_z, with the range of validity is specified by $\alpha > 1/2$ and Q_b[nC] < E_0[MV/m]/10, as extensively discussed elsewhere[7]. The formulae reported here correspond to the particular case $\phi = \pi/2$ examined in Ref. 7, augmented with the focusing effects of the solenoidal magnetic field.

Let us define the beam energy γ_1 and γ_2 at the first and second iris location, namely $\gamma_1 = 1 + \pi\alpha/2$ and $\gamma_2 = 1 + 3\pi\alpha/2$. The solenoid field starts at $z_b = \lambda/8$ and extends to due $z_c = (1/8 + 5/4)\lambda$, and the transverse forces imparted to beam electrons during acceleration, are represented by a defocusing RF term Δp^{RF}, a defocusing space charge term Δ_{SC} and a focusing term Δ_B produced by the magnetic field of the solenoid. Expressed in terms of two auxiliary quantities, $\mu = \sum_1^{\infty} a_n$ ($\mu = 1$ for an ideal first harmonic field for which $a_1 = 1$, $a_3 = a_5 = \ldots = 0$) and $\mu_{SC} = \frac{\pi I \zeta(A)}{4 I_0 \gamma'^2 \sigma_r^2}$., they take the form

$$\Delta p^{RF} = \mu\left[1 + \mu - \frac{\mu \log(\gamma_1)}{\gamma_1 - 1}\right] - \frac{\eta(1 - (\alpha/4!)^2)\log(\gamma_2)}{8}\left[1 + \mu - \frac{\mu \log(\gamma_1 \sqrt[3]{\gamma_2})}{2(\gamma_1 - 1)}\right] \quad \text{(A.1)}$$

$$\Delta_{SC} = (\mu + \mu_{SC})\left[1 - \frac{\log(\gamma_2)}{\gamma_2 - 1}\right] \quad \text{(A.2)}$$

$$\Delta_B = b^2 \log^2(\gamma_2 / \gamma_b)/2 \quad \text{(A.3)}$$

In practice the RF term, which is a function only of α, is nearly constant with a slight oscillation around the value 1.06 all over the range $1/2<\alpha<3$, as shown in Ref.7, for the case of $\mu=\eta=1$. In the following we will therefore take $\Delta p^{RF}=1.06$.

Finally, the beam exit conditions σ_2 and σ_2' are:

$$\sigma_2=\sigma_r\left(1+\Delta_{SC}-\Delta_B\right) \tag{A.4}$$

$$\sigma_2'=\sigma_{orb}'-\frac{\gamma'}{2\gamma_2}\sigma_2 \tag{A.5}$$

where σ_2' is the secular envelope divergence, while σ_{orb}' is the actual orbit divergence

$$\sigma_{orb}'=\frac{\gamma'}{\gamma_2}\sigma_r\left(1.06+\mu_{SC}-2\Delta_B(1+\Delta_{SC}-\Delta_B)/\log(\gamma_2/\gamma_b)\right) \tag{A.6}$$

The space charge impulse factor μ_{SC} contains a geometric form factor $\xi(A)$ (see Appendix B), which depends on the bunch aspect ratio A, approximately as $\xi(A)=\dfrac{1}{2.45+1.82A^{5/4}-0.55A^{3/2}}$

According to the normalization applied in Section IV to transform the transverse beam size σ into the dimensionless quantity τ, defined as $\tau=\sigma/\sqrt{S}$ with $S=\dfrac{2I}{I_0\gamma'^2\gamma_2}$, we give here the corresponding quantities $\tau_2=\sigma_2/\sqrt{S}$ and $\dot{\tau}_2=\dfrac{\gamma_2\sigma_2'}{\gamma'\sqrt{S}}$. Using the quantity Λ defined in Section V, $\Lambda=\dfrac{I}{\gamma'^2\sigma_r^2}$, the dimensionless beam conditions τ_2 , $\dot{\tau}_2$ and $\tau_2^{\dot{o}rb}$ become:

$$\tau_2=\sqrt{\frac{I_0\gamma_2}{2\Lambda}}\left\{1+\left(\mu+\frac{\pi\zeta(A)\Lambda}{4I_0}\right)\left[1-\frac{\log(\gamma_2)}{\gamma_2-1}\right]-b^2\log^2(\gamma_2/\gamma_b)/2\right\} \tag{A.7}$$

$$\dot{\tau}_2 = \sqrt{\frac{I_0\gamma_2}{2\Lambda}}\left\{\begin{array}{l} 0.56-\frac{1}{2}\left[1-\frac{\log(\gamma_2)}{\gamma_2-1}\right]+\frac{\pi\zeta(A)\Lambda}{8I_0}\left(1+\frac{\log(\gamma_2)}{\gamma_2-1}\right)+b^2\log^2(\frac{\gamma_2}{\gamma_b})/4- \\ b^2\log(\frac{\gamma_2}{\gamma_b})\left[1+\left(\mu+\frac{\pi\zeta(A)\Lambda}{4I_0}\right)\left(1-\frac{\log(\gamma_2)}{\gamma_2-1}\right)-b^2\log^2(\frac{\gamma_2}{\gamma_b})/2\right] \end{array}\right\} \quad \text{(A.8)}$$

$$\tau_2^{\dot{o}rb} = \sqrt{\frac{I_0\gamma_2}{2\Lambda}}\left\{\begin{array}{l} 1.06+\frac{\pi\zeta(A)\Lambda}{4I_0}- \\ b^2\log(\frac{\gamma_2}{\gamma_b})\left[1+\left(\mu+\frac{\pi\zeta(A)\Lambda}{4I_0}\right)\left(1-\frac{\log(\gamma_2)}{\gamma_2-1}\right)-b^2\log^2(\frac{\gamma_2}{\gamma_b})/2\right] \end{array}\right\} \quad \text{(A.8-b)}$$

which are functions of only four parameters: α, A, Λ and b (recalling that γ_1, γ_2, and γ_b are functions only of α).

Let us assume now that the first half cell may be different, in length, from an exact quarter of RF wavelength, so that the first iris is located at $z_1 = (1+d)\lambda/4$ and the second one at $z_2 = z_1 + \lambda/2$. Following the calculations by Serafini (L.Serafini, in *Advanced Accelerator Concepts*, 45 (AIP, 1993)), we can express the beam energies γ_1 and γ_2 in the form

$$\gamma_1 = 1+\frac{\pi\alpha}{2}\left[1+\frac{5}{4}d-\left(\frac{5}{16}+\frac{\pi^2}{24}\right)d^2\right] \;;\; \gamma_2 = 1+\frac{3\pi\alpha}{2}\left[1+\frac{5}{12}d-\left(\frac{5}{2}+\frac{\pi^2}{3}\right)\frac{d^2}{24}\right], \quad \text{(A.9)}$$

while the term Δp^{RF} and Δ_{SC} become

$$\Delta p^{RF} = \left\{\begin{array}{l} \mu\left[1+\mu-\frac{\mu\log(\gamma_1)}{\gamma_1-1}\right]- \\ \frac{\eta\left(1-(\alpha/4!)^2\right)\log(\gamma_2)}{8}\left[1+\mu-\frac{\mu\log(\gamma_1\sqrt[3]{\gamma_2})}{2(\gamma_1-1)}\right] \end{array}\right\}\left(1+\frac{2}{3}d-\frac{d^2}{2}\right) \quad \text{(A.10)}$$

$$\Delta_{SC} = \left[\mu(1+0.2475d)+\mu_{SC}\right]\cdot\left[1-\frac{\log(\gamma_2)}{\gamma_2-1}\right]. \quad \text{(A.11)}$$

The actual orbit divergence at the second iris, σ'_{orb} , is found to be

$$\sigma'_{orb} = \frac{\gamma'}{\gamma_2}\sigma_r\left[1.06\left(1+\frac{2}{3}d-\frac{d^2}{2}\right)+\mu_{SC}-2\Delta_B(1+\Delta_{SC}-\Delta_B)/\log(\gamma_2/\gamma_b)\right] \qquad \text{(A.12)}$$

Finally, the dimensionless beam exit conditions τ_2 and $\tau_2^{\dot{o}rb}$ at the second iris are:

$$\tau_2 = \sqrt{\frac{I_0\gamma_2}{2\Lambda}}\left\{1+\left(\mu(1+0.2475d)+\frac{\pi\zeta(A)\Lambda}{4I_0}\right)\left[1-\frac{\log(\gamma_2)}{\gamma_2-1}\right]-\right\}, \text{ and} \qquad \text{(A.13)}$$
$$b^2\log^2(\gamma_2/\gamma_b)/2$$

$$\tau_2^{\dot{o}rb} = \sqrt{\frac{I_0\gamma_2}{2\Lambda}}\left\{\begin{array}{l}1.06\left(1+\frac{2}{3}d-\frac{d^2}{2}\right)+\frac{\pi\zeta(A)\Lambda}{4I_0}- \\ b^2\log(\frac{\gamma_2}{\gamma_b})\left[1+\left(\mu(1+0.2475d)+\frac{\pi\zeta(A)\Lambda}{4I_0}\right)\left(1-\frac{\log(\gamma_2)}{\gamma_2-1}\right)-\right]\end{array}\right\}. \qquad \text{(A.14)}$$
$$b^2\log^2(\frac{\gamma_2}{\gamma_b})/2$$

APPENDIX B

The transverse rms kick due to the space charge field is represented by the factor μ_{SC} in Eq. A.2 for a Gaussian distribution of transverse size σ_r and longitudinal σ_z, with total charge Q_b. As extensively reported elsewhere [7], μ_{SC} is calculated by averaging (in the rms sense) the transverse electric field component of the bunch E_r^{sc} (at rest in the laboratory frame),

$$E_r^{sc}(r,\zeta)=\frac{Q}{2\varepsilon_0(2\pi)^{3/2}\sigma_r^2\sigma_z}r\int_0^\infty dx\frac{e^{-\frac{1}{2}\left[\frac{r^2}{\sigma_r^2(1+x)}+\frac{\zeta^2}{\sigma_z^2(1+A^2x)}\right]}}{(1+x)^2\sqrt{(1+A^2x)}} \tag{B.1}$$

over the charge density distribution $\rho(r,\zeta)=\frac{Q_b}{(2\pi)^{3/2}\sigma_r^2\sigma_z}\exp\left[-\frac{r^2}{2\sigma_r^2}-\frac{\zeta^2}{2\sigma_z^2}\right]$, to get

$$\mu_{SC}=\frac{\pi\gamma_2}{2E_0\gamma'\sigma_r}\left[\frac{1}{2Q}\iiint_{V_\infty}\rho(r,\zeta)E_r^2(r,\zeta)rdrd\phi d\zeta\right]^{1/2} \tag{B.2}$$

which can be cast in the form $\mu_{SC}=\frac{\pi I\xi(A)}{4I_0\gamma'^2\sigma_r^2}$, with

$$\xi(A)=\left\{\int_0^\infty dx_1\int_0^\infty dx_2\frac{\left[(1+A^2x_1)(1+A^2x_2)+2+A^2(x_1+x_2)\right]^{-1/2}}{\left[(1+x_1)(1+x_2)+2+x_1+x_2\right]^2}\right\}^{\frac{1}{2}}. \tag{B.3}$$

$\xi(A)$ can be represented within 1 % error in the range $0\le A\le 6$ by the function

$$\xi(A)=\frac{1}{2.45+1.82A^{5/4}-0.55A^{3/2}}. \tag{B.4}$$

Since μ_{SC} is actually the global rms space charge kick on the bunch, we are interested in evaluating the kick μ_{SC}^+ applied on the central bunch slice, located at ζ=0, and the one μ_{SC}^- applied to the slice located at $\zeta=\sigma_z$. These are given by

$$\mu_{SC}^+=\frac{\pi\gamma_2}{2E_0\gamma'\sigma_r}\left[\sqrt{\frac{\pi}{2}}\frac{\sigma_z}{Q}\int_0^{2\pi}d\varphi\int_0^\infty\rho(r,0)E_r^2(r,0)rdr\right]^{1/2}, \text{ and} \tag{5.5}$$

$$\mu_{SC}^{-}=\frac{\pi\gamma_2}{2E_0\gamma'\sigma_r}\left[\sqrt{\frac{\pi}{2}}\frac{\sigma_z}{Q}\int_0^{2\pi}d\varphi\int_0^{\infty}\rho(r,\sigma_z)E_r^2(r,\sigma_z)rdr\right]^{1/2}, \tag{5.6}$$

which can be cast in the form $\mu_{SC}^{+}=\frac{\pi I\xi^{+}(A)}{4I_0\gamma'^2\sigma_r^2}$ and $\mu_{SC}^{-}=\frac{\pi I\xi^{-}(A)}{4I_0\gamma'^2\sigma_r^2}$, with

$$\xi^{+}(A)=\left\{\int_0^{\infty}dx_1\int_0^{\infty}dx_2\frac{\left[(1+A^2x_1)(1+A^2x_2)\right]^{-1/2}}{\left[(1+x_1)(1+x_2)+2+x_1+x_2\right]^2}\right\}^{\frac{1}{2}}, \text{ and} \tag{B.7}$$

$$\xi^{-}(A)=\left\{\int_0^{\infty}dx_1\int_0^{\infty}dx_2\frac{Exp\left[-\left(-1-1/(1+A^2x_1)-1/(1+A^2x_2)\right)/2\right]}{\left[(1+x_1)(1+x_2)+2+x_1+x_2\right]^2\left[(1+A^2x_1)(1+A^2x_2)\right]^{1/2}}\right\}^{\frac{1}{2}}. \tag{B.8}$$

It is convenient to re-define the kicks μ_{SC}^{+} and μ_{SC}^{-} in terms of re-scaled currents I^{+} and I^{-} : $\mu_{SC}^{+}=\frac{\pi I^{+}(A)\xi(A)}{4I_0\gamma'^2\sigma_r^2}$ and $\mu_{SC}^{-}=\frac{\pi I^{-}(A)\xi(A)}{4I_0\gamma'^2\sigma_r^2}$, where

$$\mathrm{I}^{+}(\mathrm{A})=\mathrm{I}\frac{2.45+1.82\mathrm{A}^{5/4}-0.55\mathrm{A}^{3/2}}{1.84+1.95\mathrm{A}^{5/4}-0.65\mathrm{A}^{3/2}}, \text{ and} \tag{B.9}$$

$$\mathrm{I}^{-}(\mathrm{A})=\mathrm{I}\frac{2.45+1.82\mathrm{A}^{5/4}-0.55\mathrm{A}^{3/2}}{3.84+1.74\mathrm{A}^{5/4}-0.34\mathrm{A}^{3/2}} \tag{B.10}$$

are valid approximations for I^{+} and I^{-} in the range $0 \le A \le 6$. At $A=1$ we have $I^{+}=1.19\cdot I$ and $I^{-}=0.71\cdot I$.

In order to calculate the geometrical form factor $g(\zeta)$ we consider here only the linear component $E_{lin}(\zeta)$ of the space charge field in Eq. B.1, *i.e.* $g(\zeta)=E_{lin}(\zeta)=\int_0^{\infty}dx\frac{e^{-\frac{1}{2}\frac{\zeta^2}{\sigma_z^2(1+\bar{A}^2x)}}}{(1+x)^2\sqrt{(1+\bar{A}^2x)}}$, which is the source of the perveance term $\kappa_s(\zeta)$ in the envelope equation; we want to study its dependence on the slice position ζ

for low aspect ratios $\overline{A} = A/\gamma$ in the rest reference frame. For highly relativistic beams, i.e. $\gamma >> 1$ the transverse space charge field dependence versus the longitudinal position ζ resembles the behavior of the charge density distribution: in fact, we have $g(\zeta) \xrightarrow[\overline{A}\to 0]{} \exp[-\frac{\zeta^2}{2\sigma_z^2}]$, as expected. For small $\overline{A}$ we approximate $g(\zeta)$ with its Taylor expansion up to second order in $\overline{A}$ around $\overline{A} = 0$, to obtain

$$g(\zeta) = e^{-\frac{\zeta^2}{2\sigma_z^2}}\left\{1+\overline{A}^2\left[\left(1-\frac{\zeta^2}{\sigma_z^2}\right)\left(\frac{1}{2}+\log\overline{A}\right)-1\right]\right\} + O\left(\overline{A}^4\right) \qquad \text{(B.11)}$$

FIGURE CAPTIONS

1. Emittance and envelope evolution for a slightly mismatched beam ensemble beginning with a minimum beam size and vanishing correlated emittance, in linearized limit.

2. (a) Envelope, and (b) emittance evolution of 1300 MHz RF photoinjector design, from PARMELA multiparticle simulation.

3. Schematic cross section in the (r,z) plane of a typical RF multi-cell cavity of a photoinjector gun: the RF field distribution on-axis is plotted together with the electric field lines of the $TM_{010-\pi}$ mode in use for electron acceleration.

4. Beam envelopes through two different 10+1/2 cell RF guns (ν_{RF}=2.856 GHz $E_0 = 100$ MV/m upper diagram, ν_{RF}=1.3 GHz $E_0 = 45$ MV/m lower diagram). Dashed lines give the secular orbits analytically predicted, while solid lines are numerical simulation results.

5. Beam envelopes through a 10+1/2 cell L-band RF gun ($E_0 = 45$ MV/m, I=200 A, Q_b=4 nC) at different amplitudes B_0 (in kG) of the solenoid magnetic field.

6. Operating diagram in the (α, A) plane for an indefinitely long multi-cell Photo-Injector.

7. Parameter b_s , plotted as a function of α, at some values of the bunch aspect ratio A, for an indefinitely long multi-cell Photo-Injector.

8. Current density J plotted (solid lines) versus the cathode peak field E_0 [MV/m], at different RF frequencies (indicated in MHz), for a multi-cell Photo-Injector operated in the

emittance correction regime. The dashed lines show the limit of maximum J for two different bunch lengths.

9. Cathode spot size σ_r, plotted versus the cathode peak field E_0 [MV/m], at different RF frequencies, for a multi-cell Photo-Injector operated in the emittance correction regime.

10. (a) Envelope and (b) emittance evolution as predicted by the operating diagram in Fig.6, obtained by numerical integration of the envelope equation, with and without solenoid focusing applied (solid and dashed lines respectively).

11. Description of a bunched beam via two representative slices in the trace space (r,r').

12. Schematic drawing of the phase space of a photoinjector beam rms matched to an invariant envelope. The offset phase space area is a Liouvillian invariant.

13. (a) Envelope and emittance evolution of the beam in the TTF-FEL photoinjector as obtained from PIC simulation. The analytical prediction of the correct invariant envelope in this case is shown for comparison in (b).

14. Plot of the function $f(\nu_c') = \int_{e^{-\nu_c'^2/2}}^{1} dx/\sqrt{\nu_c'^2 + 2\ln x}$ (dots): the solid line gives a fit of the function, namely $g(\nu_c') = \frac{1.09\,\nu_c'}{1.69 + \nu_c'^2} + 0.423\,\nu_c' e^{-0.296\nu_c'^2}$.

15. Operating diagram in the (α, A) plane for a short (1+1/2 cell) Photo-Injector.

16. Parameter b^{opt} , plotted as a function of α, at some values of the bunch aspect ratio A.

17. Current density J plotted as a function of the cathode peak field E_0 [MV/m], at different RF frequencies, for a short Photo-Injector operated in the emittance correction regime.

18. Cathode spot size σ_r, plotted versus the cathode peak field E_0 [MV/m], at different RF frequencies, for a short Photo-Injector operated in the emittance correction regime.

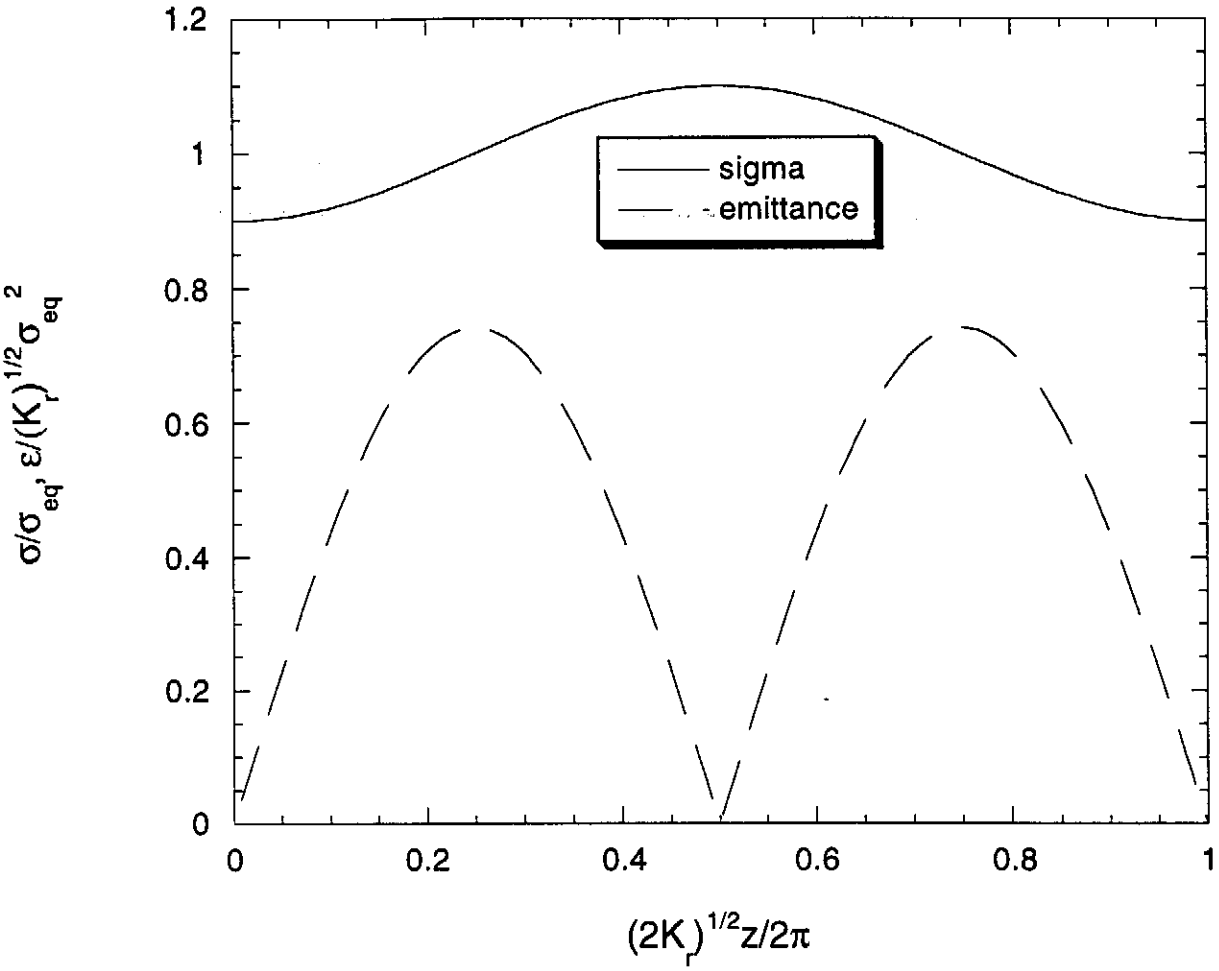
1.2
1
0.8
0.6
0.4
0.2
0
0
0.2
0.4
0.6
0.8
1
sigma
emittance
σ/σeq, ε/(Kr)1/2σeq 2
(2Kr)1/2z/2π

FIGURE 1

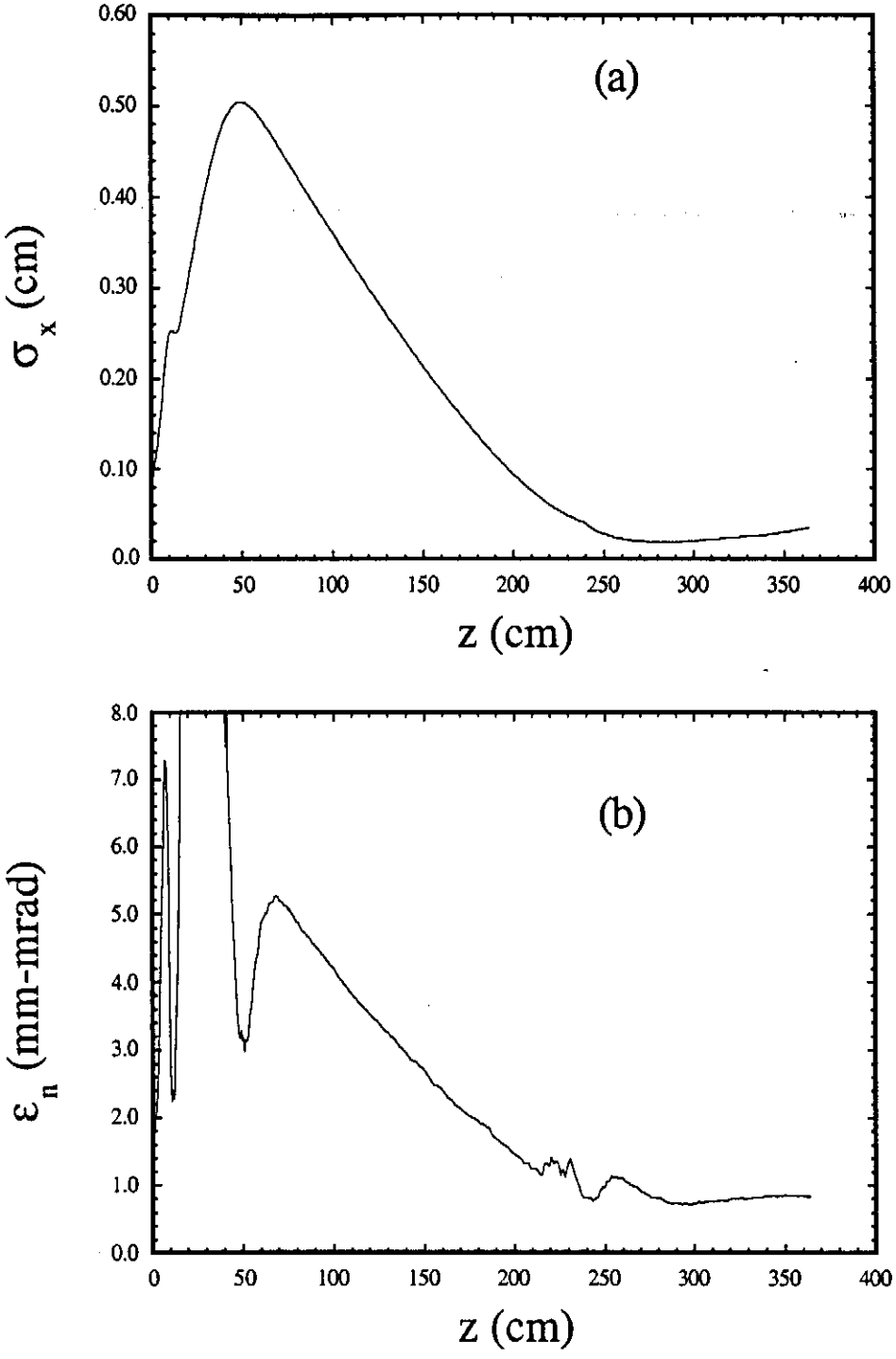
(a)
σ x (cm)
0.60
0.50
0.40
0.30
0.20
0.10
0.0
0
50
100
150
200
250
300
350
400
z (cm)
(b)
ε n (mm-mrad)
8.0
7.0
6.0
5.0
4.0
3.0
2.0
1.0
0.0
0
50
100
150
200
250
300
350
400
z (cm)

FIGURE 2

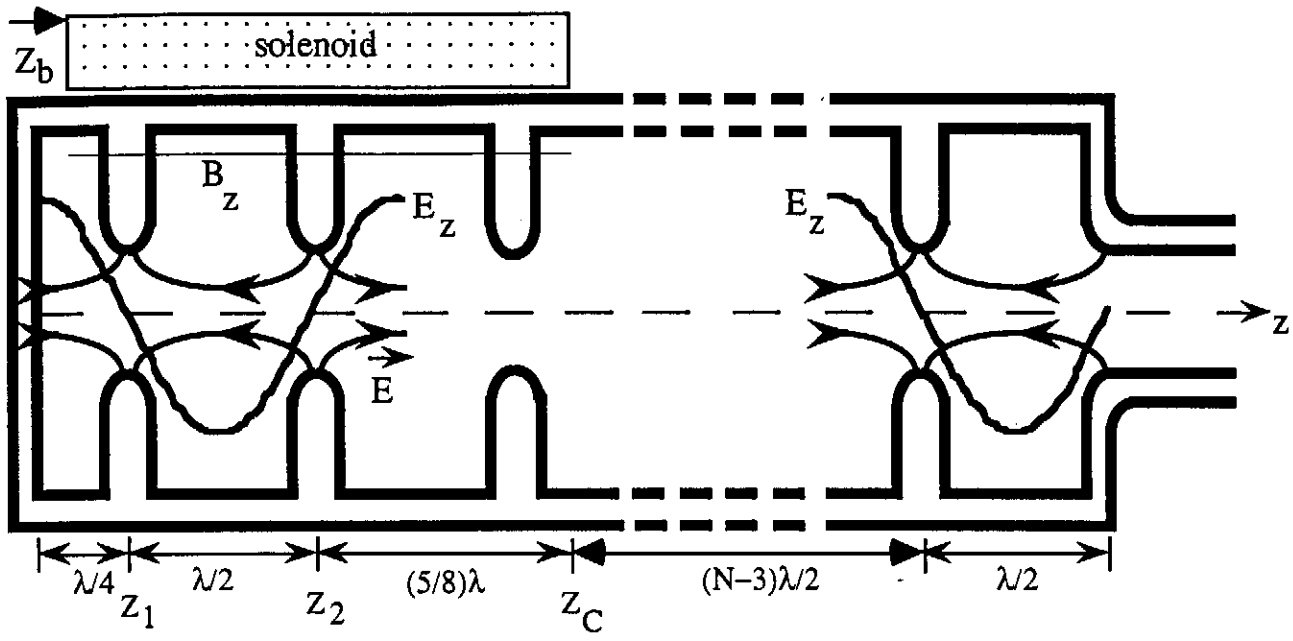

FIGURE 3

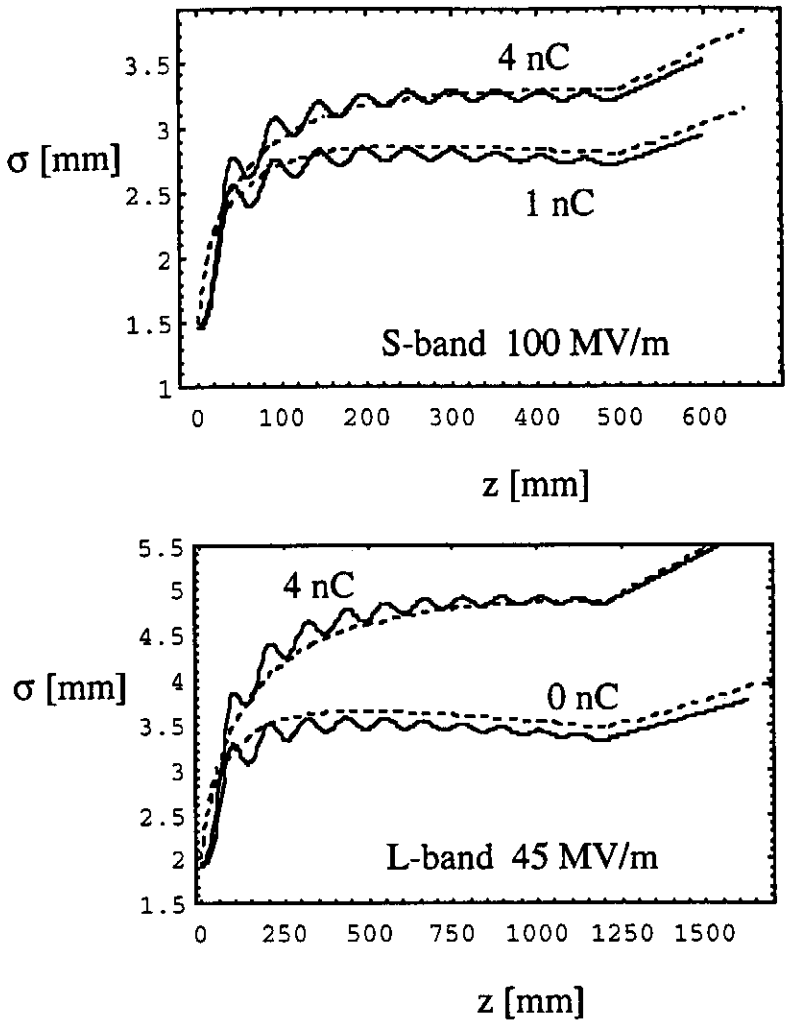

FIGURE 4

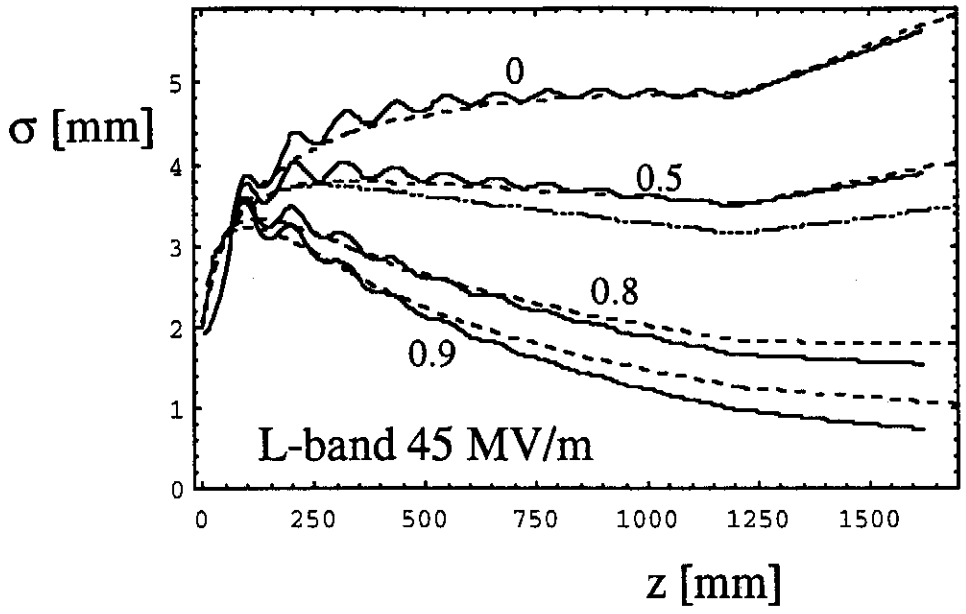

FIGURE 5

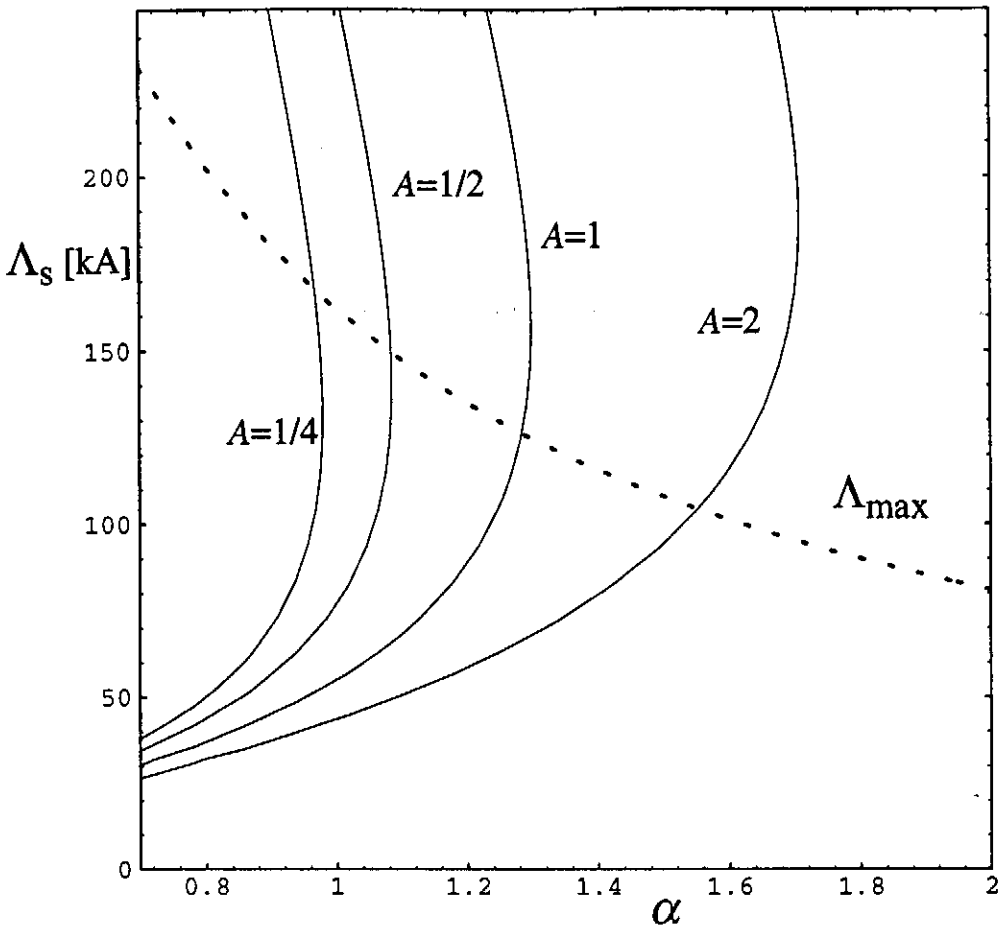
200
150
100
50
0
Λ_s [kA]
A=1/2
A=1
A=2
A=1/4
Λ_{max}
0.8
1
1.2
1.4
1.6
1.8
2
α

FIGURE 6

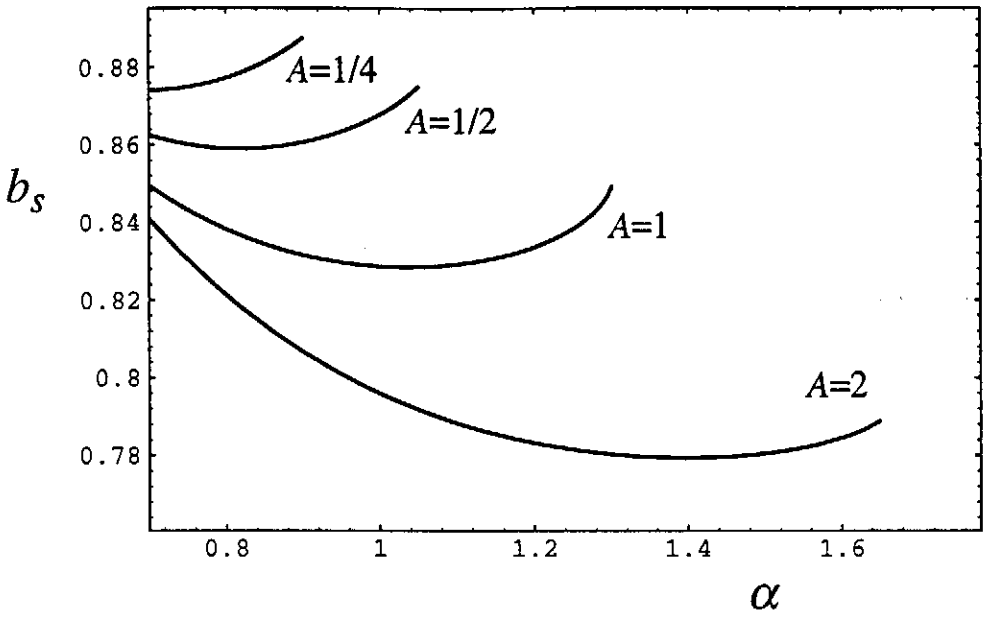

FIGURE 7

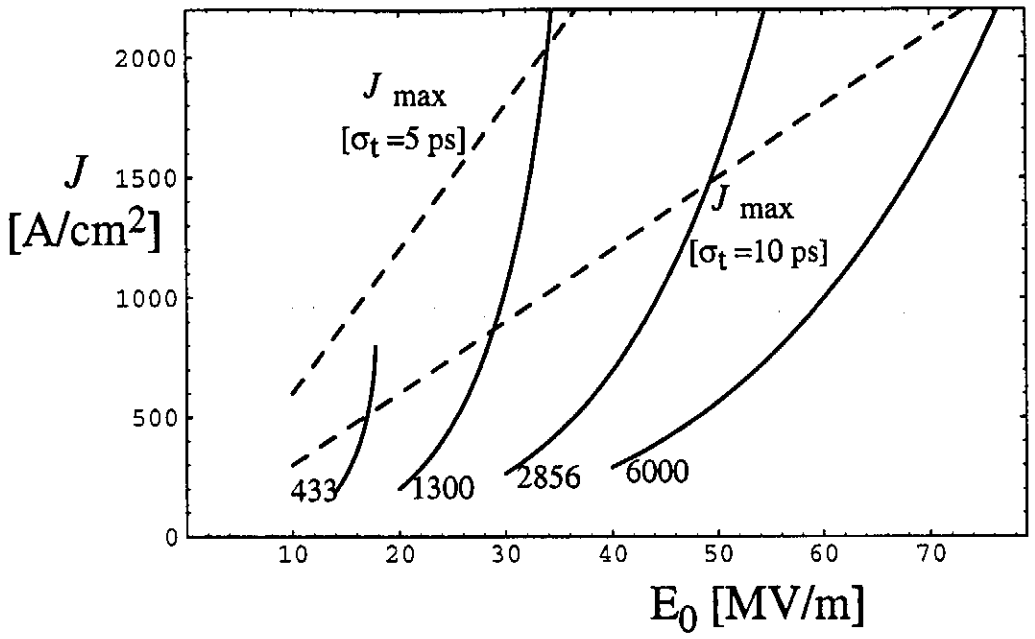
2000
1500
1000
500
0
J
[A/cm2]
J max
[σt =5 ps]
J max
[σt =10 ps]
433
1300
2856
6000
10
20
30
40
50
60
70
E0 [MV/m]

FIGURE 8

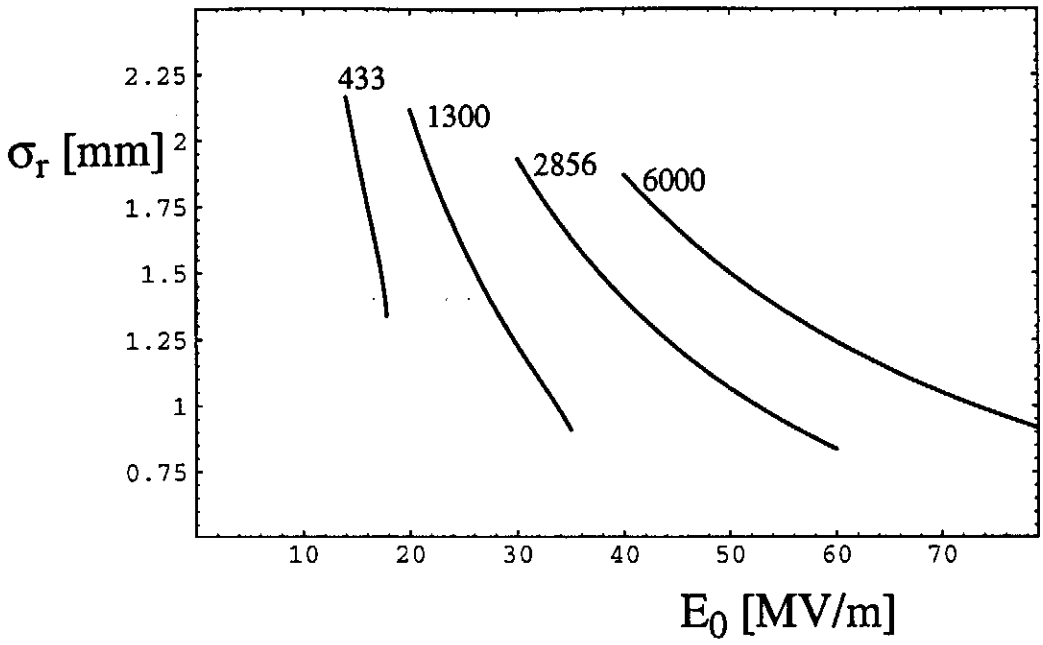
2.25
2
1.75
1.5
1.25
1
0.75
σ_r [mm]
433
1300
2856
6000
10
20
30
40
50
60
70
E_0 [MV/m]

FIGURE 9

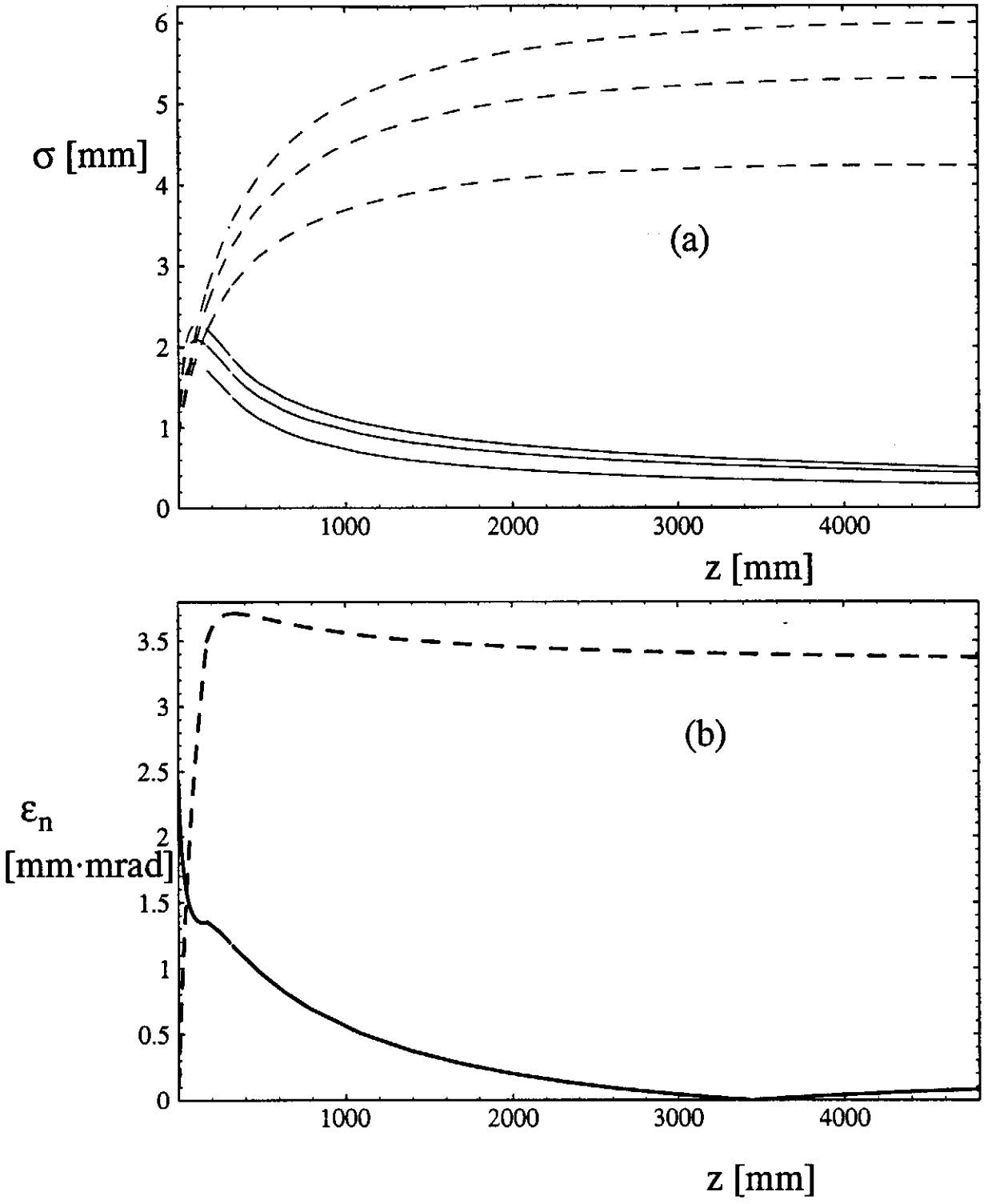
σ [mm]
6
5
4
3
2
1
0
(a)
1000
2000
3000
4000
z [mm]
εn
[mm·mrad]
3.5
3
2.5
2
1.5
1
0.5
0
(b)
1000
2000
3000
4000
z [mm]

FIGURE 10

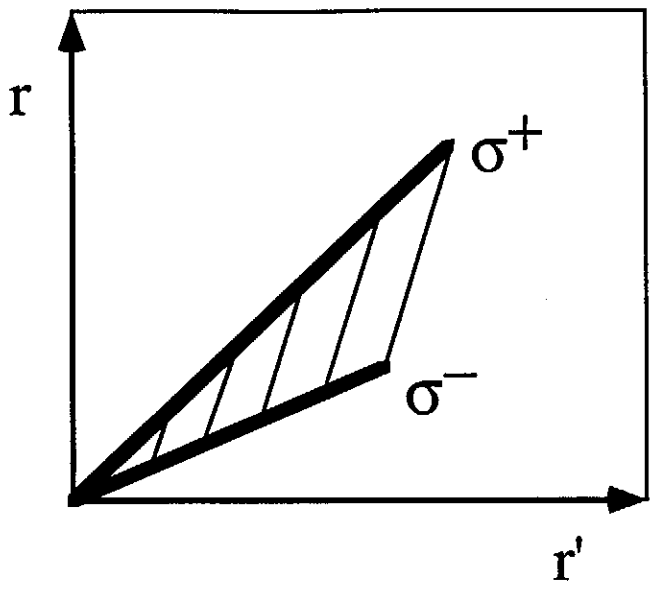

FIGURE 11

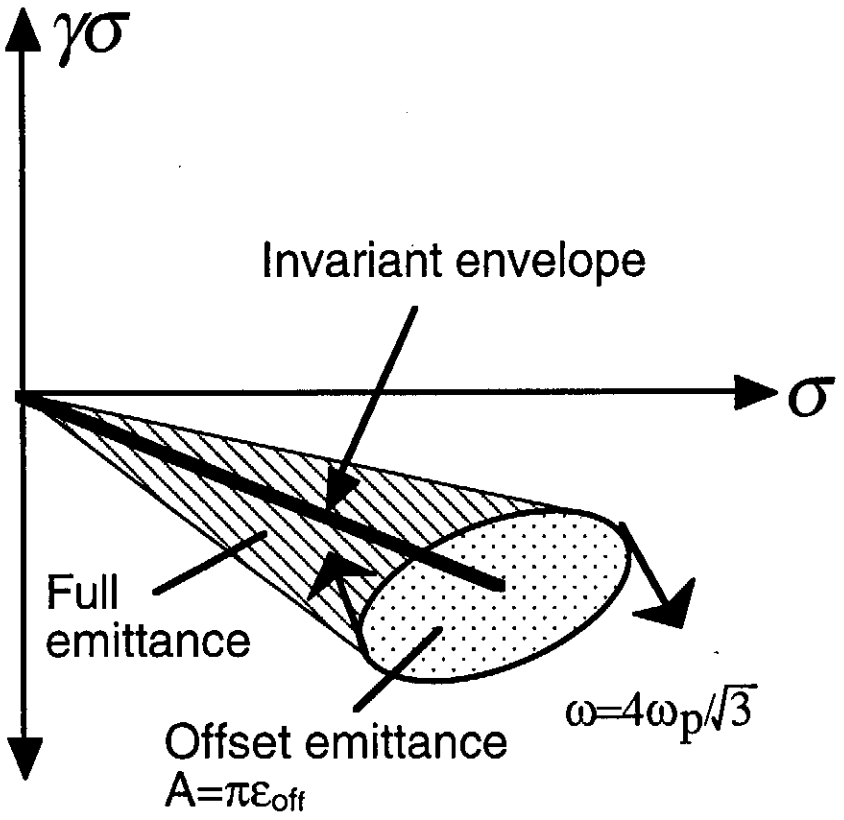
γσ
Invariant envelope
σ
Full
emittance
Offset emittance
A=πε_off
ω=4ω_p/√3

FIGURE 12

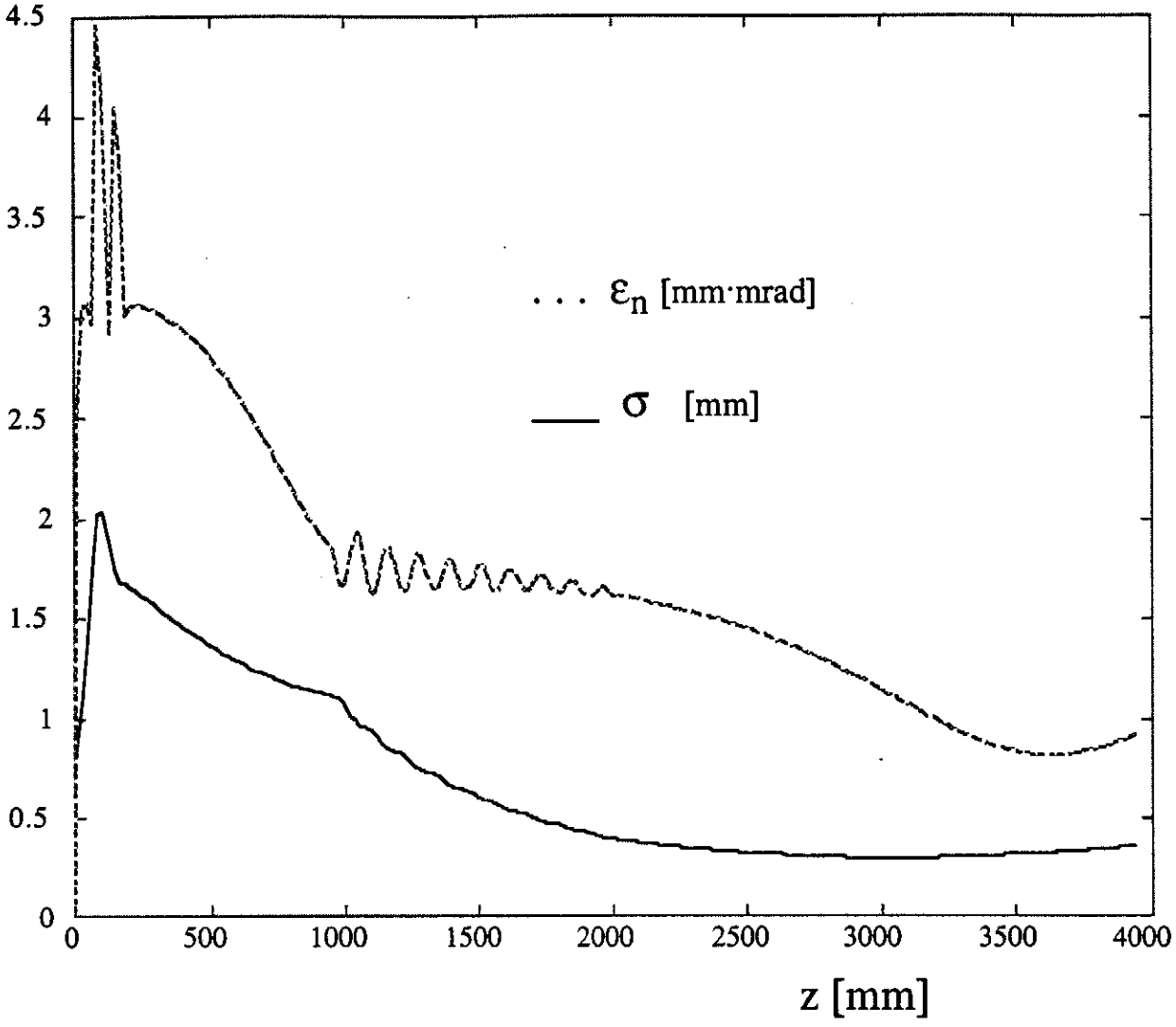
4.5
4
3.5
3
2.5
2
1.5
1
0.5
0
0
500
1000
1500
2000
2500
3000
3500
4000
z [mm]
. . . ε_n [mm·mrad]
___ σ [mm]

FIGURE 13a

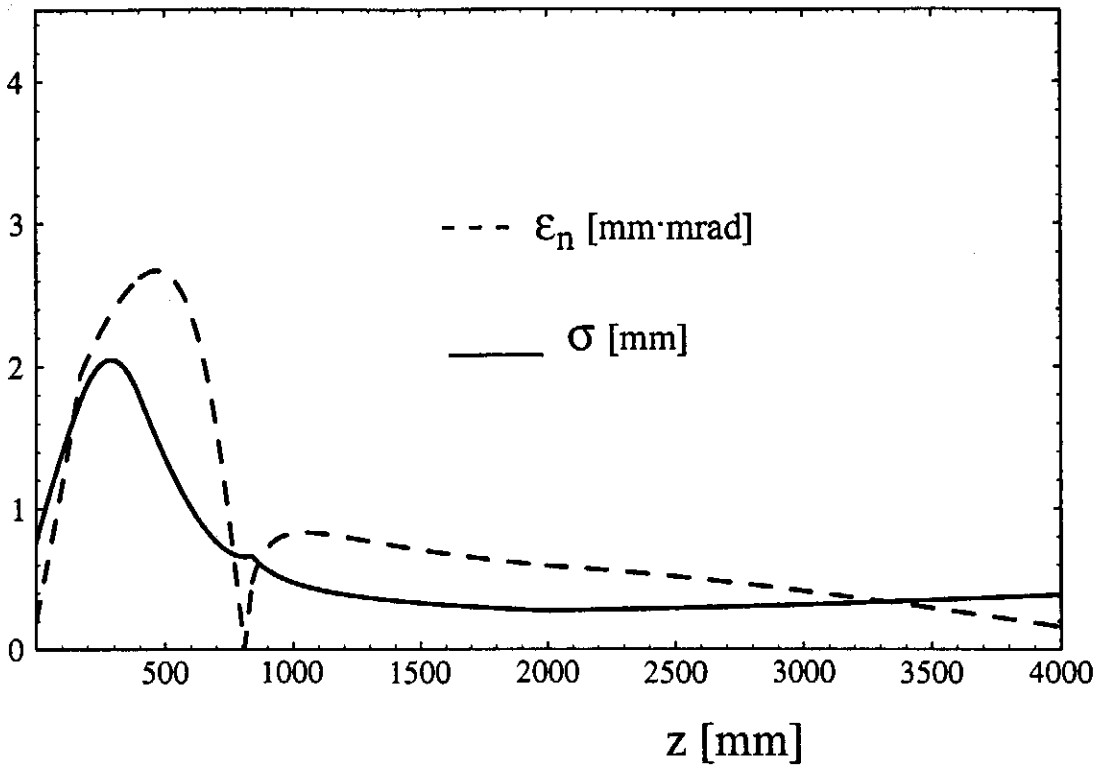
4
3
2
1
0
ε_n [mm·mrad]
σ [mm]
500
1000
1500
2000
2500
3000
3500
4000
z [mm]

FIGURE 13b

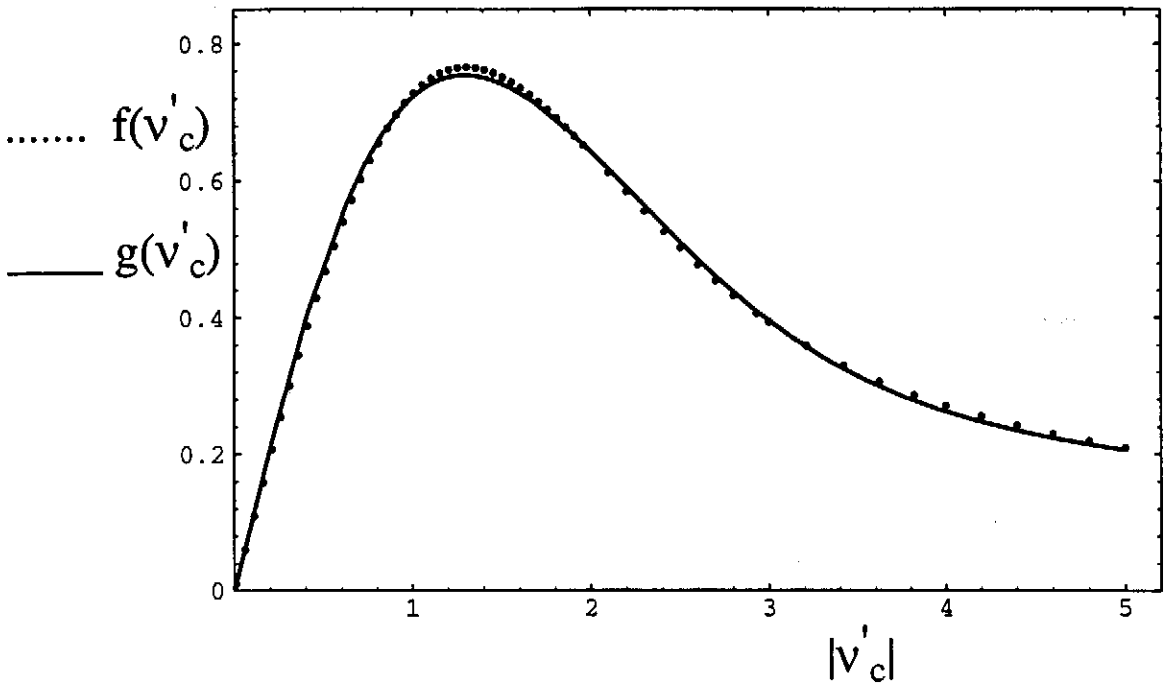

FIGURE 14

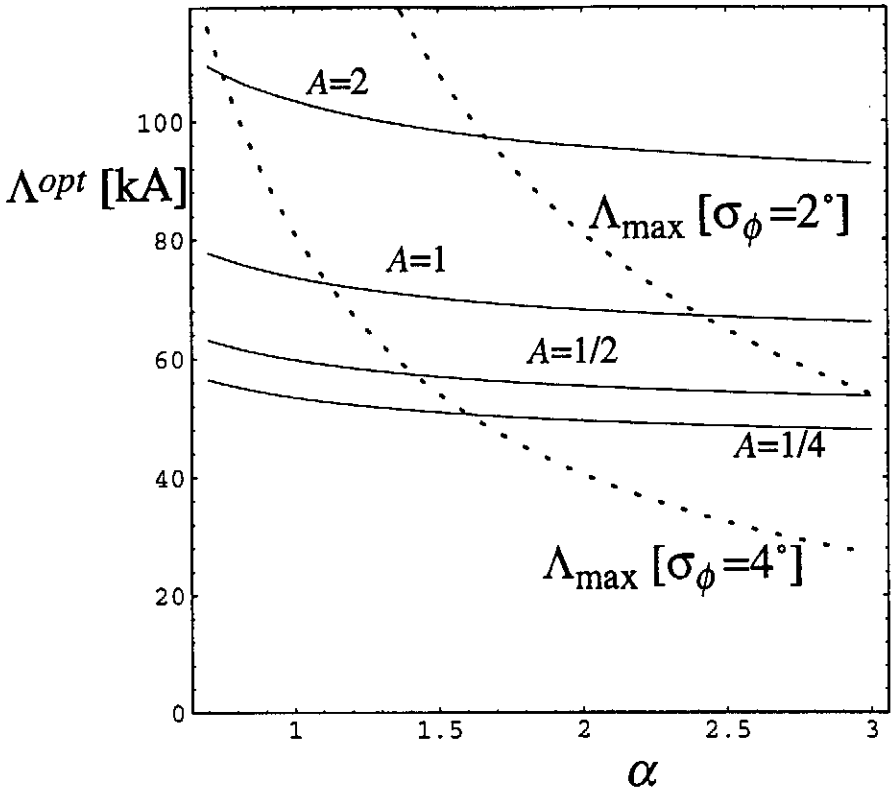
A=2
A=1
A=1/2
A=1/4
Λ_{max} [σ_ϕ=2°]
Λ_{max} [σ_ϕ=4°]
Λ^{opt} [kA]
100
80
60
40
20
0
1
1.5
2
2.5
3
α

FIGURE 15

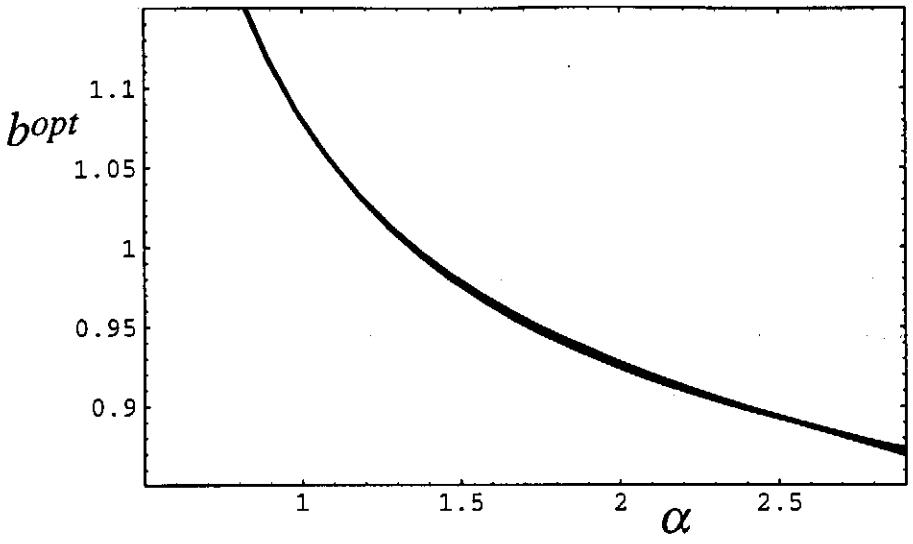

FIGURE 16

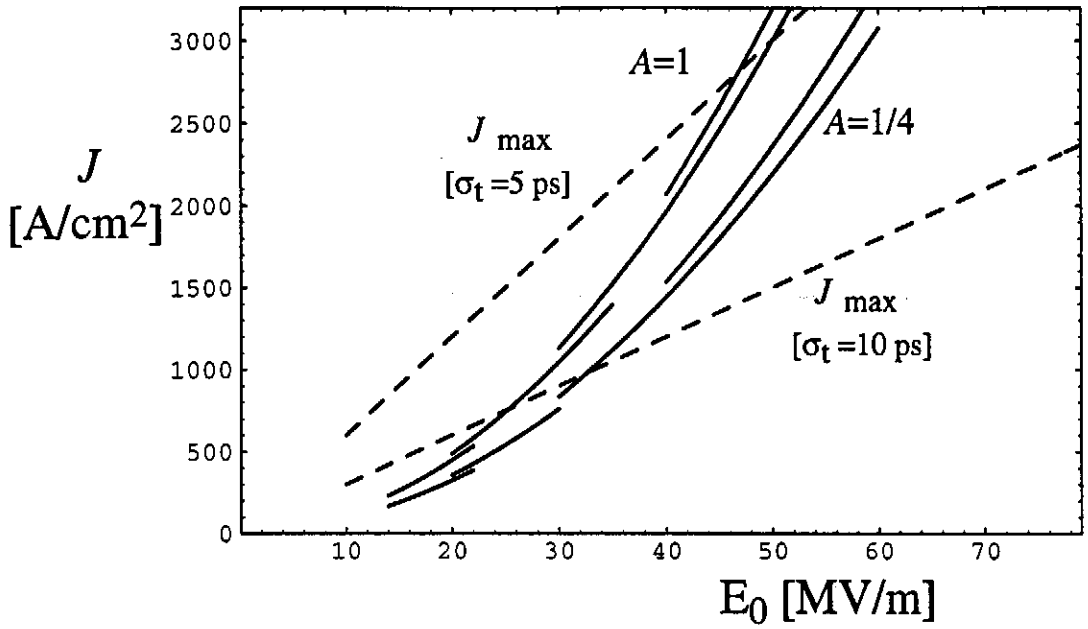
3000
2500
2000
1500
1000
500
0
J
[A/cm2]
A=1
A=1/4
J max
[σt =5 ps]
J max
[σt =10 ps]
10
20
30
40
50
60
70
E0 [MV/m]

FIGURE 17

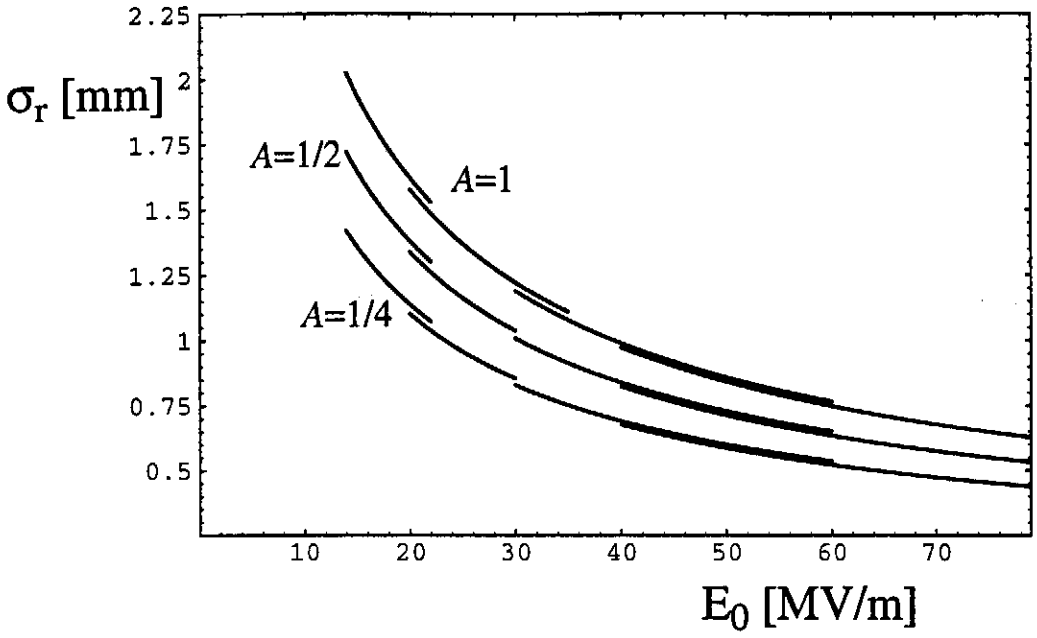

FIGURE 18